Progress in Oceanography 148 (2016) 1–25

Contents lists available at ScienceDirect

Progress in Oceanography

journal homepage: www.elsevier.com/locate/pocean

North Atlantic Ocean OSSE system development: Nature Run evaluation and application to hurricane interaction with the Gulf Stream

Vassiliki H. Kourafalou [a,*], Yannis S. Androulidakis [a], George R. Halliwell Jr. [b], HeeSook Kang [a], Michael M. Mehari [b,c], Matthieu Le Hénaff [b,c], Robert Atlas [b], Rick Lumpkin [b]

[a] University of Miami, Rosenstiel School of Marine and Atmospheric Sciences, Miami, FL, USA
[b] NOAA-AOML, Miami, FL, USA
[c] University of Miami, Cooperative Institute for Marine and Atmospheric Studies, Miami, FL, USA

ARTICLE INFO

Article history:
Received 21 December 2015
Received in revised form 1 September 2016
Accepted 5 September 2016
Available online 14 September 2016

ABSTRACT

A high resolution, free-running model has been developed for the hurricane region of the North Atlantic Ocean. The model is evaluated with a variety of observations to ensure that it adequately represents both the ocean climatology and variability over this region, with a focus on processes relevant to hurricane-ocean interactions. As such, it can be used as the "Nature Run" (NR) model within the framework of Observing System Simulation Experiments (OSSEs), designed specifically to improve the ocean component of coupled ocean-atmosphere hurricane forecast models. The OSSE methodology provides quantitative assessment of the impact of specific observations on the skill of forecast models and enables the comprehensive design of future observational platforms and the optimization of existing ones. Ocean OSSEs require a state-of-the-art, high-resolution free-running model simulation that represents the true ocean (the NR). This study concentrates on the development and data based evaluation of the NR model component, which leads to a reliable model simulation that has a dual purpose: (a) to provide the basis for future hurricane related OSSEs; (b) to explore process oriented studies of hurricane-ocean interactions. A specific example is presented, where the impact of Hurricane Bill (2009) on the eastward extension and transport of the Gulf Stream is analyzed. The hurricane induced cold wake is shown in both NR simulation and observations. Interaction of storm-forced currents with the Gulf Stream produced a temporary large reduction in eastward transport downstream from Cape Hatteras and had a marked influence on frontal displacement in the upper ocean. The kinetic energy due to ageostrophic currents showed a significant increase as the storm passed, and then decreased to pre-storm levels within 8 days after the hurricane advanced further north. This is a unique result of direct hurricane impact on a western boundary current, with possible implications on the ocean feedback on hurricane evolution.

1. Introduction

This study is motivated by the need to build a rigorous framework for evaluating the contribution of different components of ocean observing systems on coupled atmosphere-ocean hurricane models. Observing System Simulation Experiments (OSSEs) provide such a framework, as they can quantify the impact of specific observations on improving forecast skill. They can thus help evaluate and optimize existing observing platforms or quantify impacts on forecasts using data from future observational designs. An ocean OSSE framework prototype has been developed by the Ocean Modeling and OSSE Center (OMOC; http://cimas.rsmas.miami.edu/omoc.html) in Miami and was first evaluated in the Gulf of Mexico (Halliwell et al., 2014, 2015). The novelty of this ocean OSSE system is that it follows the rigorous criteria that have long been applied on realistic atmospheric OSSEs (e.g. Atlas, 1997; Atlas and Emmitt, 2008) to produce credible impact assessments. The system includes two models that need to be substantially different, in terms of overall set-up and attributes. The first one is a high resolution, state-of-the-art free-running model, able to represent both the ocean climatology and variability over the study area. It is appropriately called "Nature Run" (NR) and must be evaluated with observations to establish its realism. The second model ("Forecast Model", FM) is data assimilative and is purposely given different attributes from the NR, with typically lower spatial resolution. These different attributes introduce differences with the NR, considered as errors, which mimic the differences existing between the actual ocean and operational ocean model simulations, and which are to be corrected through the assimilation of

* Corresponding author.
E-mail address: vkourafalou@rsmas.miami.edu (V.H. Kourafalou).

http://dx.doi.org/10.1016/j.pocean.2016.09.001
0079-6611/

observations. The NR model is the source of "synthetic" observations, which are suitably simulated from this model (in terms of frequency and spatial distribution with realistic errors added) to represent all available observations (existing and planned), including the observing system under evaluation. These synthetic observations are then assimilated into the FM where data denial experiments are performed by withholding observations from the system under evaluation, to quantify the impact they have on reducing FM errors. The OMOC prototype framework for OSSEs includes comparison to identical Observing System Experiments (OSEs), where the observations that are assimilated are actual ocean observations (Kourafalou et al., 2015; Oke et al., 2015). The OSSE/OSE pairs must be shown to be compatible, to ensure that the OSSE system will produce unbiased impact assessments. This compatibility was initially demonstrated in the Gulf of Mexico (Halliwell et al., 2014), and has also been demonstrated for the present Atlantic Domain in a companion paper (Halliwell et al., 2016).

Both OSSEs and OSEs evaluate observing systems with respect to specific phenomena of interest. The NR model development leads to: (a) an integral component of this framework of observational design, optimization and impact assessment and (b) a data evaluated, free-running model that is reliable for use in process oriented studies (which cannot be performed under possible biases and potential shocks introduced by the data assimilation in analysis and forecast models). The overarching objective of this study is to develop and evaluate a high resolution NR model for the North Atlantic Ocean, with a focus on the hurricane region over the western Atlantic basin. We concentrate on hurricane impacts; therefore, we (a) choose a model domain that covers the extended hurricane region (from the Caribbean Sea and the Gulf of Mexico to the Northeast U.S. coast, Fig. 1); (b) address a process of interaction between hurricane activity and ocean variability. Further system evaluation (FM evaluation and OSE-OSSE comparisons) is presented in Halliwell et al. (2016).

The North Atlantic hurricane record begins in 1851 and is the longest among global records (Landsea et al., 2004). Only one tropical storm, in 2004, has ever been recorded in the Southern Atlantic Ocean. The vast majority (95%) of the Atlantic hurricane activity (major storms of Saffir-Simpson categories 3, 4 and 5) occurs between August and October with a peak in early to mid-September (Landsea, 1993). This is also true for hurricanes of categories 1, 2 (87%) and tropical storms (78%) in the same period. It is noted that 80% of the intense hurricanes originate close to Africa (Landsea, 1993), while the most severe and catastrophic Atlantic hurricanes in history have been recorded over the model domain depicted in Fig. 1. The costliest hurricane of all times was Katrina in 2005, followed by Sandy in 2012. Superstorm Sandy claimed over 200 lives in 6 countries (Diakakis et al., 2015), caused massive destruction valued at 75 billion USD and had the uniqueness of seriously impacting coastal areas in high latitudes. This motivated us to extend the NR model domain (Fig. 1) substantially north of the "classic" hurricane land impact region of the Caribbean Sea and Gulf of Mexico.

The interaction of hurricanes with the ocean is an important aspect of the overall hurricane evolution and a challenging component of hurricane forecasting. Hurricanes draw energy from the ocean and may cool the sea surface by several °C, with stronger winds producing faster cooling and upwelling within cyclonic ocean cells bringing cooler deep waters near the surface (Leipper and Volgenau, 1972; Price, 1981; Emanuel, 1999; Walker et al., 2005). These effects of SST cooling beneath storms provide a negative feedback that tends to reduce the heat (enthalpy) flux from ocean to atmosphere and eventually limit storm intensity (Schade and Emanuel, 1999; Bender et al., 2007; Lloyd and Vecchi, 2011; Scoccimarro et al., 2011). The stratification, along with vertical structure and heat content of the upper ocean, exert a strong influence on deepening and cooling of the mixed layer (which can reach 100–150 m in strong storms) and thus on the strength of this negative feedback (Price, 2009; Jaimes and Shay, 2015). Other parameters of the upper ocean, such as low salinity barrier layers, formed usually near large river discharges, may alter upper ocean stratification to the point that it reduces mixed layer deepening and cooling rates (Grodsky et al., 2012; Androulidakis et al., 2016).

Furthermore, Tropical Cyclones (TCs) play an important role on the evolution and structure of almost all major circulation patterns

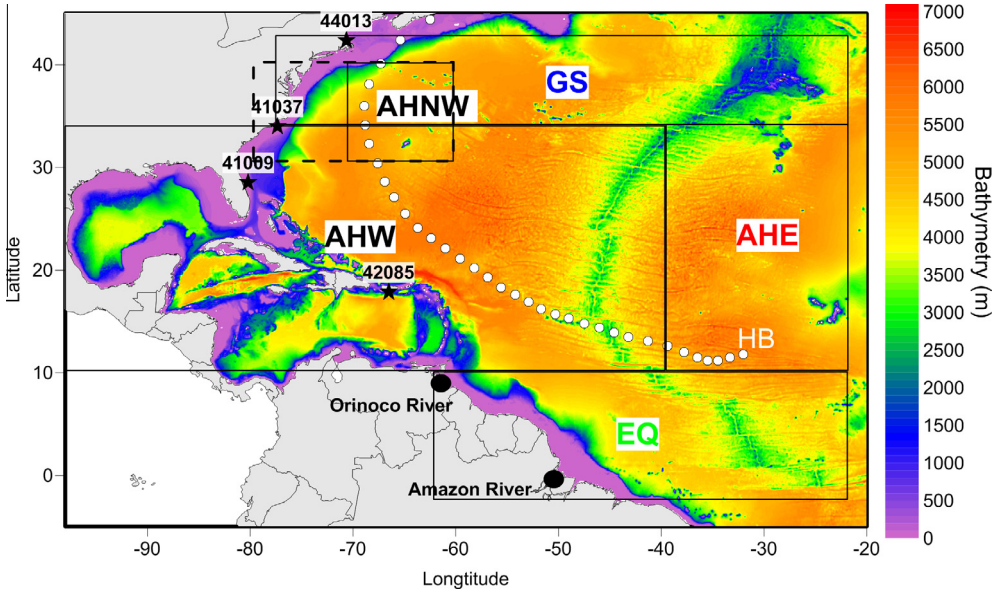

Fig. 1. Bathymetry (m) of model domain and Atlantic Hurricane Western (AHW), Atlantic Hurricane Eastern (AHE), Gulf Stream (GS), Equatorial (EQ), and Atlantic Hurricane Northwestern (AHNW) sub-regions. The extended AHNW region (used in Figs. 16–18) is indicated with a dashed line. Black stars indicate the positions of NDBC buoys (stars are below the buoy numbers): #42085 in the Caribbean Sea; #41009 and #41037 over the Southeast U.S. Continental Shelf; #44013 over the Mid-Atlantic Bight. White circles mark the passage of Hurricane Bill (HB) in summer of 2009 (circles are every 6 h at the hurricane core). The Orinoco and Amazon River discharge locations are indicated with big black dots. The Pacific Ocean is masked with white color and is not included in the simulations. (For interpretation of the references to colour in this figure legend, the reader is referred to the web version of this article.)

of the North Atlantic hurricane region. Hurricane Wilma's entrance into the Gulf of Mexico increased the volume and the heat transport through the Yucatan Channel, warming the upper ocean around the Loop Current, which then influenced the storm's fate (Oey et al., 2006). Such oceanic variability and interaction with the atmosphere may also have important impacts on hurricane evolution. Warm core eddies can intensify the hurricane activity (e.g. Loop Current Eddy with Hurricane Opal in 1995; Bosart et al., 2000), while cold core eddies may weaken TCs (e.g. cyclonic eddies around the Loop Current interacting with Hurricane Ivan in 2004; Walker et al., 2005). The interactions between oceanic eddies and hurricanes are not limited to the changes in heat content, but also include dynamical interactions with relative vorticity patterns associated with the eddy field (Jaimes and Shay, 2015). A statistical view is provided by Bright et al. (2002), who examined all TCs that crossed the Gulf Stream during 1944–2000. They found that intense storms (above category 3) and those occurring early in the Atlantic hurricane season (before August) are more likely to intensify after interacting with this warm oceanic current. However, examples of late season intensification also exist. A specific study is given by Nguyen and Molinari (2012) for Hurricane Irene (1999), which intensified during passage along the northwestern edge of the warm Gulf Stream, with wind speeds significantly increasing from 33.4 to 48.9 m/s and the storm's translation speed accelerating from 10 to 18 m/s within 18 h. Another late season major hurricane that significantly intensified over the Gulf Stream is Hurricane Sandy (2012), a historically unique case of strong intensification at mid-latitude, partially attributed to the storm's track relative to the Gulf Stream (Galarneau et al., 2013). However, no previous studies have examined if a major western boundary current experienced variability directly linked to a hurricane passage. In this study we will explore such a unique interaction, focusing on the study case of Hurricane Bill (2009; HB) and the Gulf Stream. The process study objective is to examine if and how the hurricane passage influenced the Gulf Stream evolution.

Our NR model development extends previous numerical modeling studies, with different resolution scales and model types, carried out for the North and equatorial Atlantic basin over the past several decades. A simulation of the general circulation of the North Atlantic Ocean was first carried out using a thermodynamic primitive equation model in order to investigate the role of eddies in circulation and their interactions with thermodynamic processes (Bryan and Holland, 1989). The Hybrid Coordinate Ocean Model (HYCOM) was implemented for the first time over the study region in a horizontal resolution of 0.9° by Chassignet et al. (2003) in order to evaluate the use of the hybrid vertical coordinate system in ocean modeling. A North Atlantic 1/12° HYCOM simulation, which used 26 vertical layers and assimilation of satellite measured Sea Surface Height (SSH, Chassignet et al., 2007), provided boundary conditions to a Gulf of Mexico HYCOM simulation at 1/25° resolution in order to investigate the oceanographic processes generated by Hurricane Ivan (Zamudio and Hogan, 2008). Beckmann et al. (1994), based on simulations with different horizontal resolutions over the North Atlantic domain, showed that although coarse resolution can describe many features of the large-scale circulation, the higher resolution may significantly improve the variability of the simulated ocean fields. Moreover, various higher resolution simulations were also developed over sub-regions of the North Atlantic hurricane region (i.e. Caribbean Sea, Gulf of Mexico, South Florida), in order to investigate with more detail specific regional circulation and physical processes (Jouanno et al., 2008; Le Hénaff et al., 2012; Le Hénaff and Kourafalou, 2016; Kourafalou and Androulidakis, 2013; Kourafalou and Kang, 2012). In this study, we employ the HYCOM code and have chosen a regionally high resolution (1/25°, ie. 0.04°) for the NR model North Atlantic Ocean domain (abbreviated as "ATL"). Therefore, we will also refer to the NR model as ATL-HYCOM 0.04° to distinguish from any previous applications of HYCOM over the Atlantic Ocean.

Following this introductory part, Section 2 describes the work methods and tools, comprising of *in situ* observations, satellite data, hurricane meteorological data and model characteristics and set-up. The ATL-HYCOM 0.04° simulation results and evaluation of the North Atlantic hurricane region NR model is presented in Section 3. Section 4 discusses a model application related to a process study of hurricane and ocean interaction over the Gulf Stream. Section 5 provides a summary of concluding remarks.

2. Model and data description

2.1. The North Atlantic Hurricane Region HYCOM model set up

The Hybrid Coordinate Ocean Model (HYCOM; https://hycom.org/) code was initially developed to produce a real-time global and basin-scale ocean hindcast, nowcast, and prediction system in the context of the Global Ocean Data Assimilation Experiment (GODAE), an international collaboration for ocean forecasting activities (Chassignet et al., 2007). The HYCOM unique hybrid vertical discretization (Bleck, 2002) is an important feature in regions with combination of waters that are either deep (isopycnal coordinates), coastal and shelf (sigma coordinates), very shallow or within the mixed near-surface (cartesian coordinates). Detailed information about the HYCOM model can be found in the HYCOM manual (Bleck et al., 2002) as well as in numerous studies, where several aspects of the model were described, evaluated and calibrated during the last decade (Halliwell, 2004; Kara et al., 2005; Winther and Evensen, 2006; Chassignet et al., 2007).

There are several implementations of HYCOM over the North Atlantic Ocean (i.e. Chassignet et al., 2003; Halliwell, 2004; Simon and Bertino, 2009; Mehra and Rivin, 2010). In this study, a simulation for the North Atlantic hurricane region (defined as: 98.0°W to 20.0°W and 5.0°S to 45.0°N; Fig. 1) has been performed with a HYCOM configuration of about 3–4 km horizontal resolution (ATL-HYCOM 0.04°), which is twice the previously available highest resolution applications; vertical resolution is 35 hybrid layers. For the initial and boundary conditions, the model uses the global HYCOM analysis (GLB-HYCOM), which has a 0.08° horizontal resolution and 32 vertical hybrid layers (https://hycom.org/global). The simulation period is September 2008 to 31 December 2015. This start time was chosen because an upgrade to the global HYCOM analysis was implemented at that time, which significantly reduced errors and biases in the analysis product.

We commenced the study of model results on 1 January 2009, to allow a few months for the free run to evolve from the initialization provided by the data assimilative global HYCOM analysis. Energetics analysis (not shown) verified that this was an adequate spin up period. Atmospheric forcing consists of the 3-hourly fields of precipitation, winds and surface heat flux from two operational U.S. Navy products: Navy Operational Global Atmospheric Prediction System (NOGAPS, available for the simulation until December 31, 2012) and NAVGEM (Navy Global Environmental Model (NAVGEM, used from January 1, 2013 to the end of the simulation). These products were obtained from the Naval Research Lab (NRL; http://www.nrl.navy.mil/) on 0.5° grids. We note here that, despite the spatial resolution of 0.5° of the atmospheric models that is quite low for a precise geographical representation of hurricanes (in particular close to their center), these models provide a smoothed representation of the storm structure, which is suitable for the overall hurricane evolution studied here. The climatological monthly discharges of 172 rivers are included with an implementation of the estuary-like area source for the Amazon River, to sim-

ulate the evolution of this major freshwater source more accurately, based on the river plume parameterization in Schiller and Kourafalou (2010). The vertical mixing scheme is the KPP (K-Profile Parameterization, described in detail in Large et al., 1994) vertical mixing scheme with double diffusion, nonlocal boundary layer mixing and critical bulk Ri of 0.45.

The model domain contains the North Atlantic hurricane region within an area situated far from open boundaries. Fig. 1 presents the bathymetry of the model domain. The boxes illustrate four sub-regions with substantially different dynamical variability, where simulation statistics will be separately analyzed: the Gulf Stream extension region (GS), the Western and Eastern parts of the North Atlantic Hurricane region (AHW and AHE), and the Equatorial region (EQ). An additional sub-region over the Atlantic Hurricane Northwestern (AHNW) area, where Hurricane Bill (August 2009; see Section 4) propagated over the Gulf Stream path, is also indicated. The AHNW and GS regions are north of 30°N, which marks the extratropical transition of TCs, as they enter mid-latitudes.

2.2. In situ observations

2.2.1. Argo data

Argo is a global array of more than 3000 free-drifting profiling floats that measure the temperature and salinity of the upper 2000 m of the ocean. All data collected by Argo floats are publically available in near real-time via the Global Data Assembly Centers (GDACs; http://www.argo.ucsd.edu). The floats measure vertical temperature and salinity profiles at 10-day intervals. The number of vertical measurements over the study domain during 2009–2014 is approximately 48,000 T/S profiles (Table 1). In particular, the largest number of measurements covered the AHW region (20,861 profiles). The specific coverage for the other regions was 13,170 (AHE); 8735 (GS), and 5077 (EQ). The mean daily number of profiles is 9.5, 6.0, 4.0 and 2.3 for AHW, AHE, GS and EQ, respectively. The largest number of available vertical measurements refers to year 2013, where the total profiles exceed 12,000 (Table 1). Only for the AHW region, the mean daily measurements are higher than 18 for 2013. The EQ region shows the fewer daily (2.3) and total (5077) Argo measurements in comparison with the other sub-regions. When normalized by area, the AHW, AHE, GS and EQ have a count of 14, 24, 13, 10 (10^{-4} km^{-2}), respectively. As the EQ maintains the lowest count, some discrepancies in the comparison with model fields can be expected in this domain (see Section 3.3.1).

2.2.2. NDBC Buoy measurements

In situ hourly temperature and salinity data were collected from four NOAA buoy stations, operated by the National Data Buoy Center (NDBC; http://www.ndbc.noaa.gov/, Fig. 1). The following stations are used (water depths provided): #44013 (64.5 m); #41037 (30 m); #41009 (40.5 m); #42085 (8 m). Station #42085 is located in the center of the AHW, over the eastern part of the Caribbean Sea. Station #41009 is located along the eastern Florida coast, over the initial pathway of the Gulf Stream in the Atlantic Ocean. More to the North, Station #41037 is located near the boundary between the AHW and GS sub-regions and Station #44013 monitors the northwestern part of the GS sub-region. The available data from the four NDBC buoys contain measurements of Sea Surface Temperature (SST) and Sea Surface Salinity (SSS), covering different periods from 2009 to 2014. These data are used to evaluate respective temperature and salinity time series, derived from the ATL-HYCOM 0.04° model simulation. All available measurements and their characteristics (measured parameters, periods and locations) are presented in Table 2.

2.2.3. The Global Drifter Program

The Global Drifter Program (GDP) maintains a global array of ~1250 satellite-tracked surface drifting buoys to provide an accurate and globally dense set of *in situ* observations of mixed layer currents, SST and Sea Level Pressure (SLP). The GDP data can be used to support research on several applications, such as ocean circulation, seasonal and inter-annual climate predictions, satellite data calibration, as well as climate research and monitoring. The drifter data used in this study are provided by the Atlantic Oceanographic & Meteorological Laboratory (AOML; http://www.aoml.noaa.gov/phod/dac/index.php) and cover all the sub-regions of the North Atlantic hurricane region model domain (Fig. 1). Herein, we use the near-surface currents (at 15 m depth) to evaluate the model performance with respect to the near-surface circulation simulations over the four Atlantic sub-regions presented in Fig. 1. The near-surface currents are calculated from satellite-tracked drogued drifter velocities on a 0.5° × 0.5° latitude-longitude grid using the methodology presented by Lumpkin and Johnson (2013).

2.2.4. GDEM climatology

The Generalized Digital Environment Model (GDEM) has served as the U.S. Navy's global gridded ocean temperature and salinity climatology for several decades. GDEM is a monthly 1/4° climatology of temperature and salinity developed by the U.S. Naval Oceanographic Office as a four-dimensional steady-state model of interpolated ocean profiles. The profile dataset for GDEM4 (Carnes, 2010) was constructed by combining profiles from the Navy's MOODS (Master Oceanographic Observation Date Set) profile archive (Bauer, 1982; Jugan and Beresford, 1991) with classified profiles removed, the WOD 2005 (World Ocean Database; Boyer et al., 2006), and delayed-mode Apex profiles calculated globally at 78 fixed depths down to 6600 m, using the piece-wise cubic interpolating polynomial interpolator. Observational data were gridded onto each depth surface over the entire domain and were objectively analyzed to a standard 1/4° grid. Values of temperature, salinity and their respective variances were calculated at all grid points. The most recent version is GDEM4; its greatest improvement compared to the previous GDEM3 dataset is in the increased size and the improved quality of the profile dataset used. A special version with enhanced data, especially for the Amazon plume region, was prepared for this study (herein named GDEM42).

Table 1
Summary and mean number of Argo profiles for all and each sub-region, and for all period and each year used in the study.

	Total number					Mean daily number				
	AHW	AHE	GS	EQ	All	AHW	AHE	GS	EQ	All
2009	1630	1561	1274	882	5347	4.5	4.3	3.5	2.4	3.7
2010	2173	1551	1338	797	5859	6.0	4.2	3.7	2.2	4.0
2011	2942	2126	1249	957	7274	8.1	5.8	3.4	2.6	5.0
2012	3094	2151	1308	738	7291	8.5	5.9	3.6	2.0	5.0
2013	6678	2569	1837	921	12005	18.3	7.0	5.0	2.5	8.2
2014	4344	3212	1729	782	10067	11.9	8.8	4.7	2.1	6.9
All	20861	13170	8735	5077	47843	9.5	6.0	4.0	2.3	5.5

Table 2
Location and period of NDBC stations (temperature and salinity data).

Station #	Location	Period
41009	28.522°N - 80.188°W	2008–2012
42085	17.86°N - 66.524°W	2013
44013	42.346°N - 70.651°W	2009–2012
41037	33.988°N - 77.363°W	2010–2014

2.3. Satellite observations

2.3.1. GHRSST data

Daily SST fields from the Group for High Resolution SST (GHRSST; https://www.ghrsst.org/) were collected in order to evaluate the ATL-HYCOM 0.04° model performance on near-surface temperature patterns. In 2002, the GODAE international project initiated the GHRSST Pilot Project to address an emerging need for more accurate high resolution SST products (Donlon et al., 2003). Satellite SST, derived from the GHRSST project, is a key observation used by forecasting and prediction systems to better represent the upper ocean circulation and thermal structure and to constrain the exchange of energy between the ocean and atmosphere. Several previous relevant studies have used GHRSST data, either to forecast hurricane intensity (e.g. Gentemann et al., 2006) or to investigate upper ocean response to hurricane activity (e.g. Samson et al., 2009). The available satellite data are daily averages and cover the entire study period from January 2009 to December 2014 on a daily basis. The spatial resolution of the SST satellite data is $0.011^\circ \times 0.011^\circ$.

2.3.2. Aquarius data

Satellite SSS data are provided by NASA's Jet Propulsion Laboratory (JPL), California Institute of Technology (Lagerloef et al., 2008, 2012; Lagerloef, 2012). The Aquarius mission was developed collaboratively between NASA and Argentina's space agency. Aquarius daily L3 SSS data (http://aquarius.nasa.gov/) are available since 25 August 2011, with daily coverage on a $1^\circ \times 1^\circ$ grid. These data have undergone extensive groundtruthing. The validation of Aquarius data with *in situ* measurements from Argo floats and moored buoys has shown that Aquarius SSS agrees well with Argo in a monthly average sense and even better with buoy data between 40°S and 40°N (Tang et al., 2014). Hernandez et al. (2014) compared SSS data from the Aquarius project and from the Soil Moisture and Ocean Salinity (SMOS) mission from the European Space Agency (ESA) with *in situ* observations over the subtropical North Atlantic region. They showed the effective gain of resolution and coverage provided by the satellite products over the interpolated *in situ* data. Gordon and Giulivi (2014) showed that the Aquarius SSS fields agree with the seasonal patterns and inter-annual evolution derived from *in situ* ocean surface observations over the North Atlantic Subtropical region from (Ships Of Opportunity Program, SOOP; Delcroix et al., 2005; Reverdin et al., 2007). In addition, satellite data from the Aquarius project were recently used in several studies over the Atlantic region. Grodsky et al. (2012) used Aquarius measurements to study the ocean response to Hurricane Katia (HK), which crossed the Amazon plume in early fall of 2011; Androulidakis et al. (2016) extended this study, using Aquarius data for mapping the Amazon plume. Gierach et al. (2013) and Grodsky et al. (2014) employed Aquarius and SMOS data in additional river plume studies. Based on the above, the Aquarius mission provides effective products to evaluate the ATL-HYCOM 0.04° model over the North Atlantic hurricane region with respect to SSS.

2.3.3. AVISO data

We use the Maps of Absolute Dynamic Topography (MADT) from AVISO, produced with support from CNES (Centre National d'Etudes Spatiales; https://cnes.fr). These data include the Sea Level Anomaly (SLA) estimated with altimeters in orbit, to which is added the Mean Dynamic Topography (MDT) that represents the time invariant part of the ocean topography, estimated by satellite and *in situ* observations. We use the AVISO data updated in 2014 (DUACS 2014), which uses the MDT CNES-CLS13 product. The MADT products have a resolution of 1/4° and are generated daily. We also use the surface geostrophic currents, derived from MADT fields and also distributed by AVISO at the same resolution and frequency. The MDT is an essential component for capturing dynamical features whose time average has intense signature, like the main oceanic currents.

3. Model results and evaluation of the North Atlantic Hurricane Region Nature Run

The free-running simulation with the ATL-HYCOM 0.04° model, described in the previous section, will be used as the Nature Run (NR) component of the North Atlantic hurricane region OSSE system. The evaluation of this simulation through comparison to observational data is an important step toward constructing a reliable OSSE system, as the NR is the model that provides "synthetic" observations for performing OSSEs. Although the actual OSSEs will be the focus of other manuscripts, we mention this utility of the simulation described herein, to stress the need for a comprehensive NR evaluation. Given that this is a free-running simulation, a statistical approach and the use of a variety of observational platforms provide a suitable methodology.

We first present an example of a qualitative comparison of 6-year mean fields (2009–2014) from the simulation and climatology fields. Fig. 2 shows the 6-year model averages for: (a) SST (compared to GDEM climatology); (b) SSS (compared to GDEM climatology); and (c) SSH (compared to AVISO MDT). The NR successfully captures the overall distribution of main features and fronts for all fields. The zonal SST differences and main SSS features in the NR, such as the high salinity pool in the subtropical gyre and the Amazon River low salinity plume, are similar to observations. The position of major currents (e.g. the Gulf Stream, including the Loop Current extension in the Gulf of Mexico) are well represented in both model SST and SSH. The following sections present quantitative comparisons of NR derived oceanic properties and observations, both for near-surface and at depth.

3.1. Evaluation of Sea Surface Temperature and Sea Surface Salinity

We first examine the NR model performance with respect to SST. The GHRSST data (see Section 2.3.1) provide high resolution SST, which makes them well suited for comparison to the high resolution NR SST fields, especially for the purpose of evaluating the NR with respect to future hurricane related studies. SST variability is an important oceanic factor in hurricane dynamics, affecting either the tracks of hurricanes or their intensity (Fisher, 1958). Although SST is not the best predictor of hurricane intensity variability, in particular compared to ocean heat content, it is an ocean parameter related to storm intensity (DeMaria and Kaplan, 1994). On the other hand, hurricanes influence the upper ocean characteristics and especially the SST with two major processes: vertical mixing, due to the hurricane's surface winds; and upwelling, due to the cyclonic surface circulation caused by the cyclonic winds within the storm. Price (1981) showed that the SST response is a contributor to hurricane strength, while upwelling causes a significant enhancement of the SST reduction in the case of a slowly moving hurricane. Therefore, the performance of the ATL-HYCOM 0.04° simulation with respect to the SST prediction is an important aspect of the evaluation of the model, especially for the purpose of

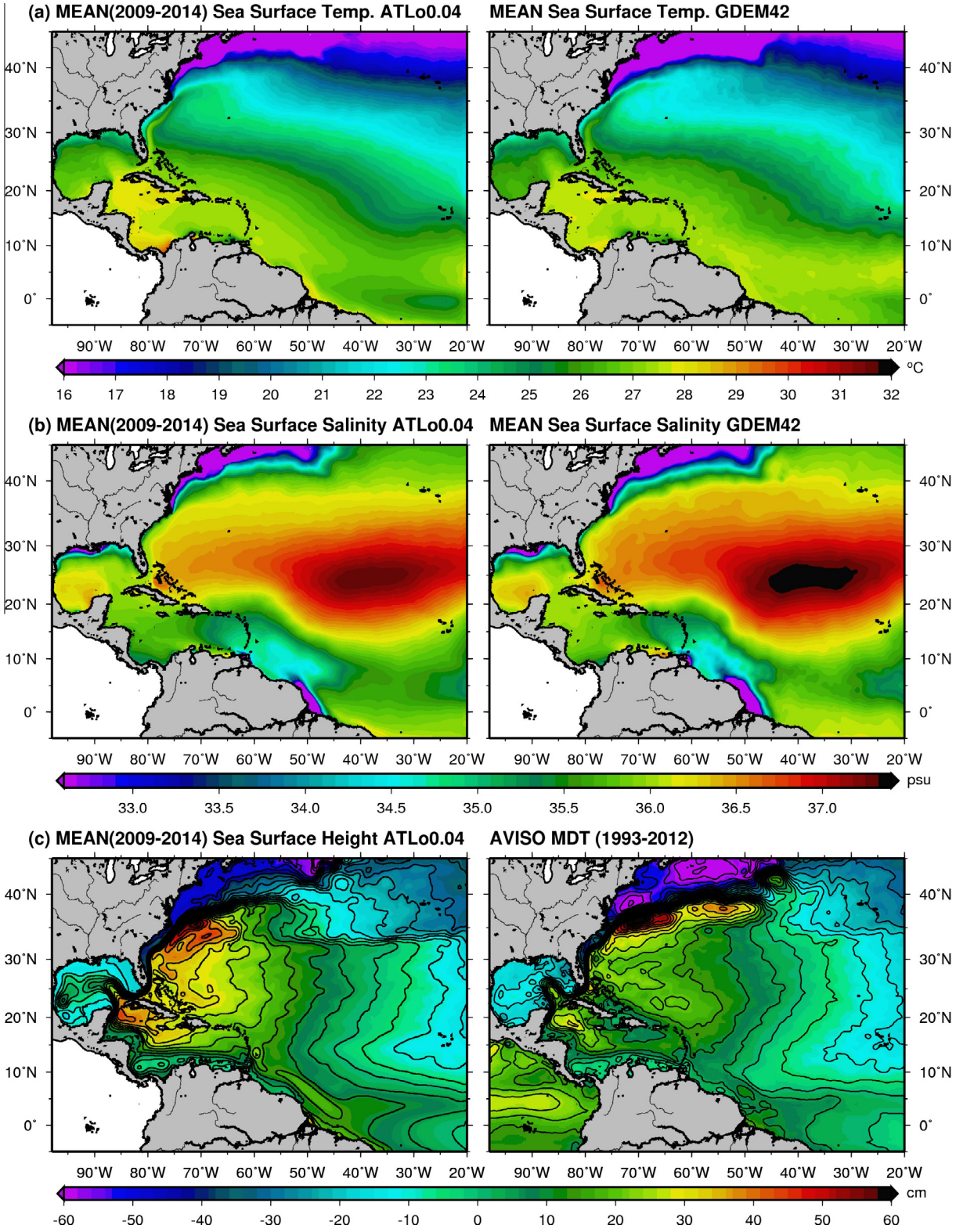

Fig. 2. Comparison of 6-year mean fields (2009–2014) calculated by the ATL-HYCOM 0.04° Nature Run model (left panels) and observations (right panels). (a): Sea Surface Temperature, compared to GDEM42 climatology; (b): Sea Surface Salinity, compared to GDEM42 climatology; (c): Sea Surface Height, compared to AVISO MDT (1993–2012, most up to date product). (For interpretation of the references to colour in this figure legend, the reader is referred to the web version of this article.)

being a reliable NR for the North Atlantic hurricane region OSSE system.

The available GHRSST satellite data cover the entire study period from January 2009 to December 2014 on a daily basis. The model evaluation is performed separately at each of the four sub-regions (Fig. 1), as these exhibit different upper ocean dynamics. We compare time series with both daily and monthly values in Fig. 3. The seasonal mean has been removed from the monthly values. The simulated SST seasonal variations agree with the observed seasonal variations at all study sub-regions, with lower values over the GS

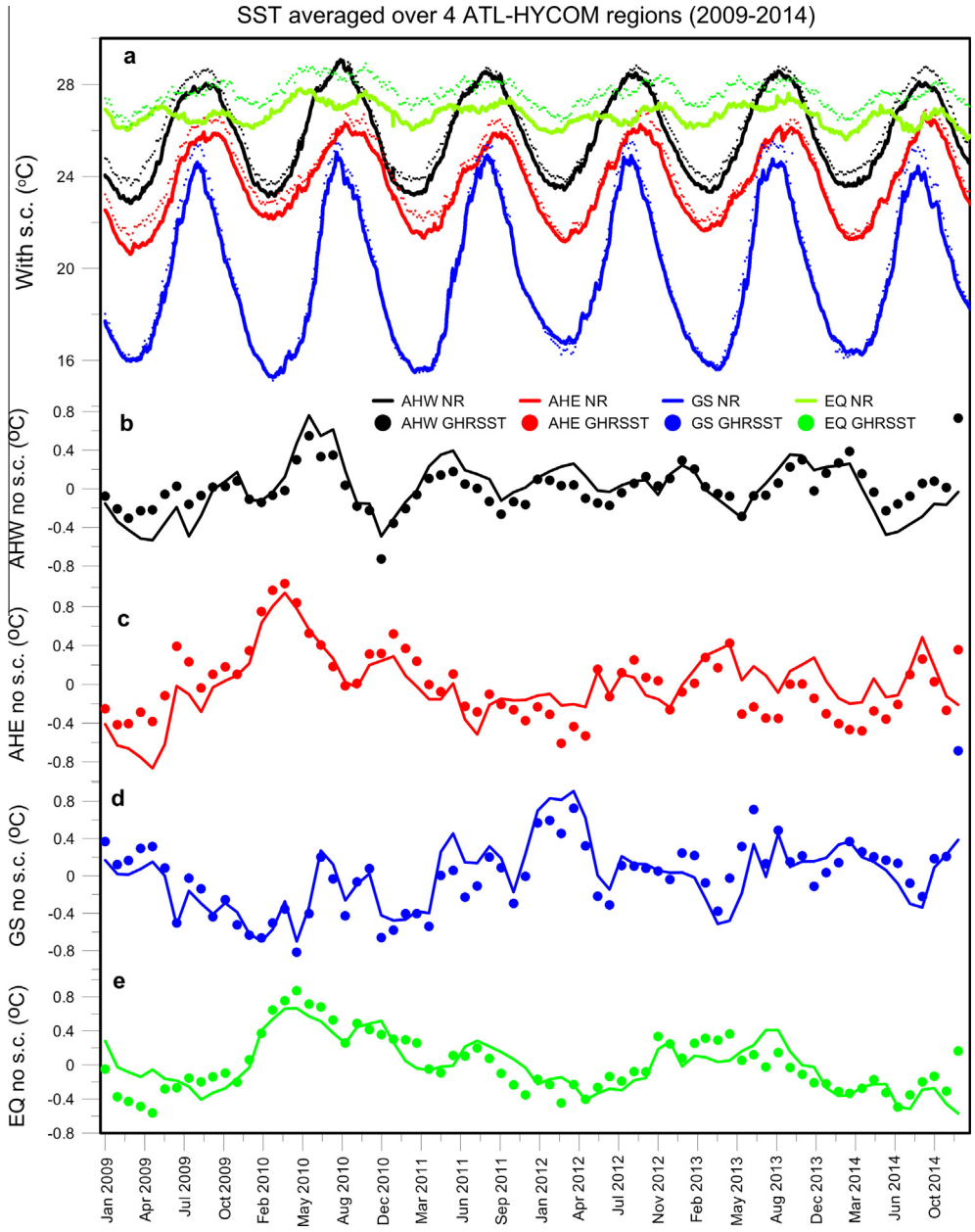

Fig. 3. Evolution of Sea Surface Temperature (°C) for the 2009–2014 study period, as derived from the NR simulation (solid lines) and GHRSST satellite data (dotted lines) averaged over all four ATL-HYCOM 0.04° sub-regions (AHW: black; AHE: red; GS: blue; EQ: green), using (a) daily values (all regions); (b)–(e) monthly values without the seasonal cycle (AHW, AHE, GS and EQ, respectively). See Fig. 1 for the definition of model sub-domains. (For interpretation of the references to colour in this figure legend, the reader is referred to the web version of this article.)

region and higher values over the EQ region (Fig. 3a). The strongest seasonal variation of SST is observed over the GS region, where the winter values from both model and observations range around 16 °C for all study years, while the summer levels may exceed 24 °C. Strong seasonality is observed in all sub-regions compared to the EQ region, where the SST levels range between 25.6–27.8 °C (2.2 °C amplitude) for NR and 26.1–28.9 °C (2.7 °C amplitude) for the GHRSST data. Moreover, the removal of the seasonal cycle from all regional time series (Fig. 3b–e) showcases the high level of agreement between the predicted and measured monthly anomalies. The time series without the seasonal cycle elucidate the temperature variation due to conditions beyond the seasonal characteristics, such as the passage of a hurricane or the appearance of a strong meteorological cold front. The largest SST anomalies (~0.8 °C), observed at all sub-regions, are usually related to atmospheric processes and broader general circulation synoptic variability, as the modulations of the Gulf Stream that affect its coverage (and, therefore, SST) in the GS region. These anomalies are well simulated by the NR model, suggesting a good performance with respect to hurricane forecasting. It is noted that the SST differences between the regions are strongly related to the seasonal effect with stronger seasonality at high latitudes compared to the equator. Although the variation without the seasonal cycle reveals similar range between all regions (−0.8 °C to 0.8 °C), several differences are also observed, due to variations in the oceanic patterns and the ocean response to atmospheric events for each region.

We employed the Willmot Skill Score W_s (Willmott, 1981) in order to quantitatively evaluate the NR model performance during the entire study period (Table 3). The calculation of W_s employs the Mean Square Error (*MSE*):

$$MSE = (\langle m\rangle - \langle o\rangle)^2 + (S_m - S_o)^2 + 2S_mS_o(1 - r_c)$$

$$W_s = 1 - \frac{MSE}{\langle(|m - \langle o\rangle| + |o - \langle o\rangle|)^2\rangle}$$

where m and o are time series of the modeled and observed variables respectively, and $\langle\rangle$ denotes temporal mean; S_m and S_o are the respective standard deviations. In addition, we also computed the Pearson coefficient r_c (Pearson, 1903) and the Root *MSE* (*RMSE*) between the simulated and observed time series of daily values for each region and year (Table 3). The majority of annual and regional *RMSEs,* derived from the NR-GHRSST comparison, are lower than 0.5 °C, while W_s is greater than 0.9 (W_s close to 1 indicates very good performance). The weakest performance is observed over the EQ region, where *RMSE* is generally higher than 0.5 °C but lower than 1 °C for all years. However, we note that the comparison of anomalies over the EQ region shows good agreement between the observed and simulated values (Fig. 3e), where the observed large monthly anomaly values (e.g. spring of 2010) were well represented by the NR simulation. The correlation coefficient between the observed and simulated values without the seasonal cycle over the EQ region is 0.80. The respective coefficients of the entire time series presented in Fig. 3b–d are 0.73, 0.77 and 0.83 for AHW, AHE and GS regions, respectively. Although the included seasonal cycle improves the correlation, the coefficients without the seasonal cycles are also quite high, indicating the satisfactory performance of the NR simulation with respect to events that do not follow the seasonal changes. The best NR performance with respect to the representation of SST, a parameter that is an important contributor to hurricane strength (Price, 1981), is observed over the two Atlantic hurricane regions (AHW and AHE), where the total *RMSEs* range around 0.5 °C for both sub-domains. This finding is very important for qualifying the ATL-HYCOM 0.04° as a suitable NR model in the context of the North Atlantic OSSE system, since the vast majority of the Atlantic hurricanes form, propagate and attenuate over these two Atlantic hurricane regions.

We now employ buoy data at specific stations from NDBC (Section 2.2.2) to evaluate time series of SST and SSS. A large number of SST (3359) and SSS (2639) NDBC observations are compared with respective values computed by the NR simulation (Fig. 4). The SST comparison reveals significantly good performance of the NR simulation with high coefficient of determination between the observed and simulated values ($R^2 = 0.93$). R^2 is a statistical measure (Steel and Torrie, 1960) that provides some information about the goodness of a model fit and how well the regression line approximates the real data points ($R^2 = 1$ indicates perfect agreement between the two time series). Scatter points are located along the identity line ($x = y$) for both low (~10 °C) and high (~30 °C) SST levels (Fig. 4a). The difference between the averaged *in situ* (22.39 °C) and simulated (22.14 °C) SST values is very small (0.25 °C). Two groups of SSS values are distinguished (Fig. 4b): a) low values with mean at 30.98, measured at station #44013, which is in the vicinity of low salinity intrusion of waters from high latitudes (see Fig. 2b) and b) higher values derived from stations #41009 (mean: 34.53), #42085 (mean: 35.22) and #41037 (mean: 35.84); see buoy locations in Fig. 1. Although the model-observation correlation with respect to the SSS is weaker than for SST, both low and high salinity values reveal high coefficient of determination ($R^2 = 0.87$) and the salinity means are very close between the simulated (~34.62) and observed (~34.31) values. The same analysis is shown in Fig. 4 for the period August–September, which is the peak of the hurricane season and also represents the study period. The agreement actually improves substantially for SSS ($R^2 = 0.91$) and remains high for SST ($R^2 = 0.93$), giving confidence that the model skill is appropriate for this study. The difference between the respective means is smaller during this 2-month period (<0.25 units).

The NR simulation adequately computed both low and high values of SST and SSS, revealing annual Pearson coefficients (r_c) that in some cases exceeded 0.90 (Table 4). In addition, the most southern available buoy (Buoy #42085) reveals very high Willmott score for SSS ($W_s = 0.93$). The mean W_s for SSS, as derived from all available buoys and years (Table 4), is equal to 0.62. The respective W_s values are significantly high for all SST comparisons; almost all SST W_s scores are higher than 0.94 (mean $W_s = 0.95$). Although the salinity W_s values are lower than the respective scores derived from SST time series, the salinity *RMSEs* are generally lower than 1. Therefore, the model performance with respect to the salinity computation is very satisfactory, based on the definition by Lewis and Allen (2009) that requires the differences between the *in situ* and model values at the surface to be below 2 units. We also note data limitations due to possible biofouling problems on the salinity sensors of the buoys (Archer et al., 2003).

The longest period of both SSS and SST continuous measurements is at station #41037 (2010–2014; Table 2). The mean monthly simulated and measured values derived from all years with #41037 data are presented in Fig. 5. The seasonal SST variation is similar between NR and *in situ* data (Fig. 5a), revealing higher values in August (28 °C) and lower ones in February (14 °C). Although the simulated variation slightly underestimates salinity (*RMSE* = 0.45–0.54; Table 4), both time series reveal a similar cycle, lagged with respect to SST, with largest and lowest values in January and May, respectively (Fig. 5b). The lower SSS levels occur late spring to early summer, following the river discharge seasonality along the East U.S. coast, which reveals high outflow levels following the spring snow melting (Kourafalou et al., 1996). The SST monthly variation follows the typical summer surface evolution at mid-latitudes with high values in mid-summer and late-summer (July–August) in agreement with satellite observations (Fig. 3a).

The NR simulated SSS variability is further compared to data from the Aquarius satellite mission (see Section 2.3.2) during the common period 2011–2014 (Fig. 6). The satellite data were averaged over the four Atlantic sub-regions and their mean monthly

Table 3
Annual and total Pearson Correlation coefficient (r_c) annual RMSE, and Willmott Skill Score (W_s) of the Sea Surface Temperature (SST) as derived from daily satellite observations (GHRSST) and NR simulations during the 2009–2014 period.

	AHW			AHE			GS			EQ		
	r_c	*RMSE*	W_s	r_c	*RMSE*	W_s	r_c	*RMSE*	W_s	r_c	*RMSE*	W_s
2009	0.99	0.58	0.98	0.99	0.72	0.96	0.99	0.55	0.99	0.49	0.94	0.50
2010	0.99	0.33	0.99	0.99	0.52	0.96	0.99	0.42	0.99	0.89	1.04	0.56
2011	0.99	0.31	0.99	0.99	0.56	0.97	0.99	0.32	0.99	0.86	0.92	0.51
2012	0.99	0.36	0.99	0.99	0.44	0.99	0.99	0.43	0.99	0.87	1.02	0.54
2013	0.99	0.45	0.99	0.99	0.33	0.99	0.99	0.76	0.99	0.96	0.91	0.55
2014	0.99	0.62	0.96	0.99	0.29	0.99	0.99	0.63	0.99	0.80	1.05	0.48
Total	0.99	0.50	0.99	0.99	0.50	0.98	0.99	0.52	0.99	0.85	0.98	0.56

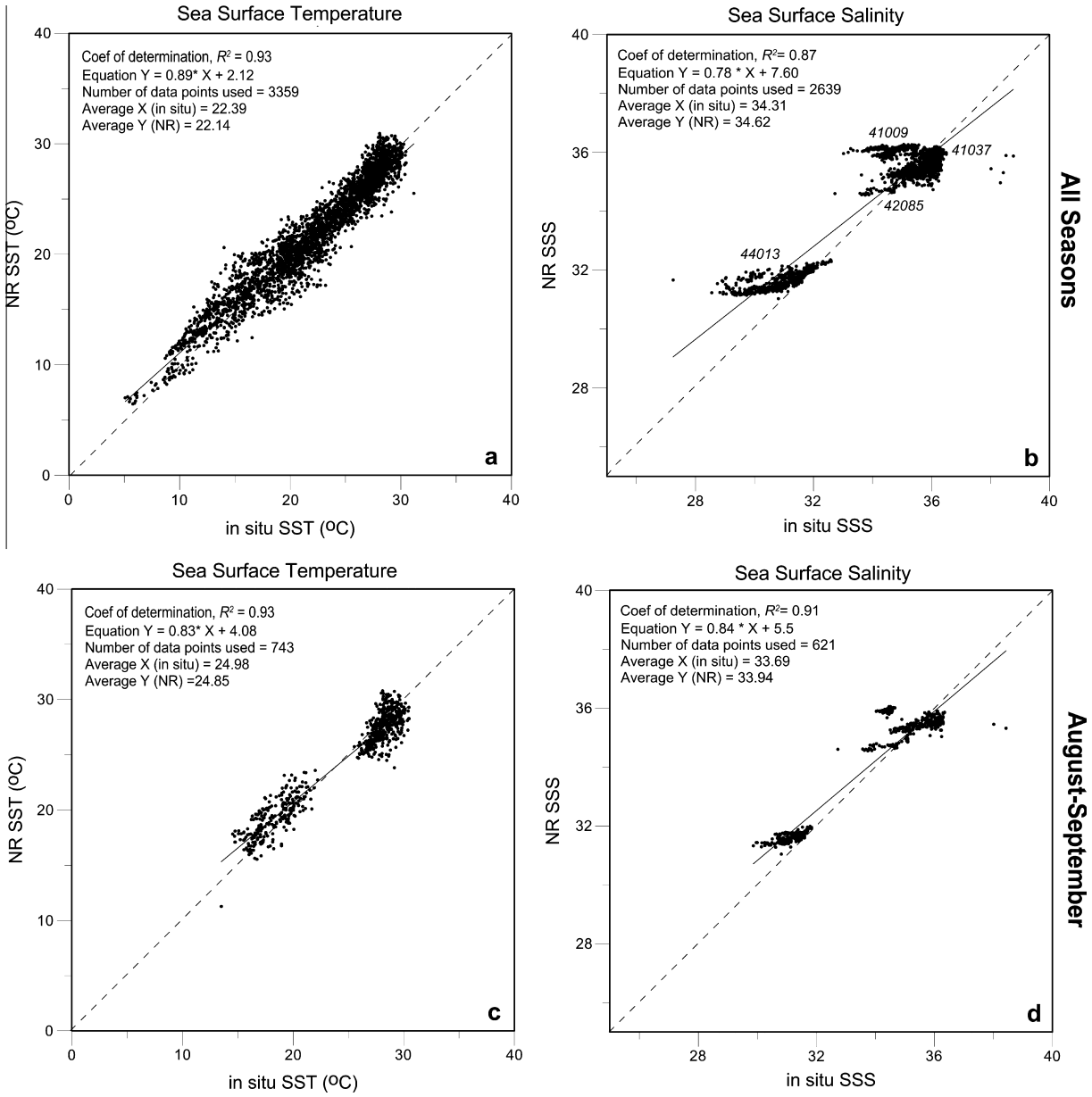

Fig. 4. Scatter diagram between all available (left) Sea Surface Temperature (SST) and (right) Sea Surface Salinity (SSS) measurements from the 4 NDBC stations and the respective simulated results from the NR experiment (specific station numbers are indicated for the two SSS groups). (a) and (b): all seasons included; (c) and (d): August–September only. The equation of the linear fit, the average annual values, the number of data points used, the residual mean square and the coefficient of determination for both parameter comparisons are also presented.

SSS evolution during the entire study period is presented in Fig. 6a. The simulated NR salinity variation ranges over similar salinity levels as the respective Aquarius monthly means. Both model and observations show the highest values over the AHE area (>36.5), while the lowest values occurred over the EQ region during summer (~35). Almost all regions show weak seasonal variations, with almost stable monthly values during the entire annual cycle. Only the EQ region reveals significant differences between the summer and the winter values, when the lowest SSS during July and August are thought to be related to the summer rainy period over the tropics and the strong Amazon-Orinoco discharges in summer months (Lentz, 1995), which may decrease the overall salinity levels. Fig. 6b presents the high seasonal variation, averaged over the EQ region during the 2011–2014 period; the good performance of the NR over the EQ region with respect to the SSS is also confirmed by the high Pearson correlation coefficient (0.72; Fig. 6) and W_s score (0.69; Fig. 6) in agreement with the high scores computed for the most southern Buoy #42085 (Table 4; Section 3.2), which is the closest to the EQ area. Despite the weakest model scores over the GS sub-region, the model performance is quite satisfactory, as all surface salinity *RMSEs* are relatively low ($\leqslant 0.4$).

3.2. Evaluation of near-surface currents

In order to investigate the NR performance with respect to the near-surface circulation, we examine the climatology of near-surface currents for the N. Atlantic region, at monthly frequency and one-half degree resolution, derived from satellite-tracked surface drifting buoy observations (see Section 2.2.3). This analysis uses quality controlled data from the GDP (Lumpkin and Johnson, 2013), extended to the period 1979–2014 for this study. The drifter

Table 4
Annual Pearson Correlation coefficient (r_c), annual *RMSE*, and Willmott skill score (W_s) between the NR experiment and Sea Surface Temperature (SST) and Salinity (SSS) measurements from 4 NDBC stations during the 2009–2014 simulation period. N/A denotes missing *in situ* data.

		#41009		#41037		#42085		#44013	
		SST	SSS	SST	SSS	SST	SSS	SST	SSS
2009	r_c	0.92	0.68	N/A	N/A	N/A	N/A	0.95	0.92
	RSME	1.68	1.25	N/A	N/A	N/A	N/A	1.49	0.95
	W_s	0.94	0.37	N/A	N/A	N/A	N/A	0.95	0.63
2010	r_c	0.94	0.36	0.95	0.59	N/A	N/A	0.93	0.45
	RSME	1.34	1.91	0.87	0.54	N/A	N/A	1.47	0.89
	W_s	0.96	0.11	0.97	0.50	N/A	N/A	0.96	0.77
2011	r_c	0.94	N/A	0.98	0.25	N/A	N/A	0.97	0.54
	RSME	1.41	N/A	1.57	0.48	N/A	N/A	1.18	1.20
	W_s	0.95	N/A	0.99	0.54	N/A	N/A	0.98	0.73
2012	r_c	0.85	N/A	0.96	0.42	N/A	N/A	0.95	0.95
	RSME	1.21	N/A	1.24	0.53	N/A	N/A	1.84	0.63
	W_s	0.90	N/A	0.98	0.60	N/A	N/A	0.94	0.73
2013	r_c	N/A	N/A	0.91	0.64	0.98	0.90	N/A	N/A
	RSME	N/A	N/A	2.15	0.45	0.84	0.33	N/A	N/A
	W_s	N/A	N/A	0.94	0.73	0.87	0.93	N/A	N/A
2014	r_c	N/A	N/A	0.96	0.53	N/A	N/A	N/A	N/A
	RSME	N/A	N/A	1.41	0.45	N/A	N/A	N/A	N/A
	W_s	N/A	N/A	0.96	0.63	N/A	N/A	N/A	N/A

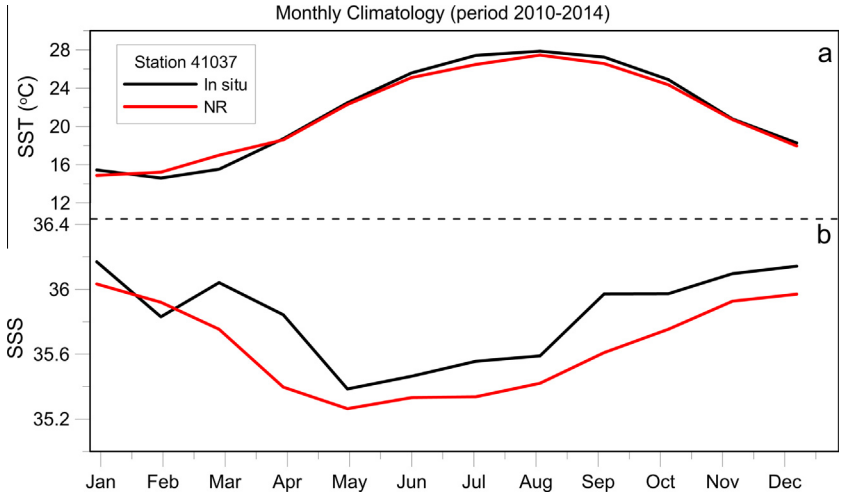

Fig. 5. Mean monthly variation of (a) Sea Surface Temperature (SST, °C) and (b) Sea Surface Salinity (SSS), derived from simulated (NR) and measured (Station #41037) time series for the period 2010–2014.

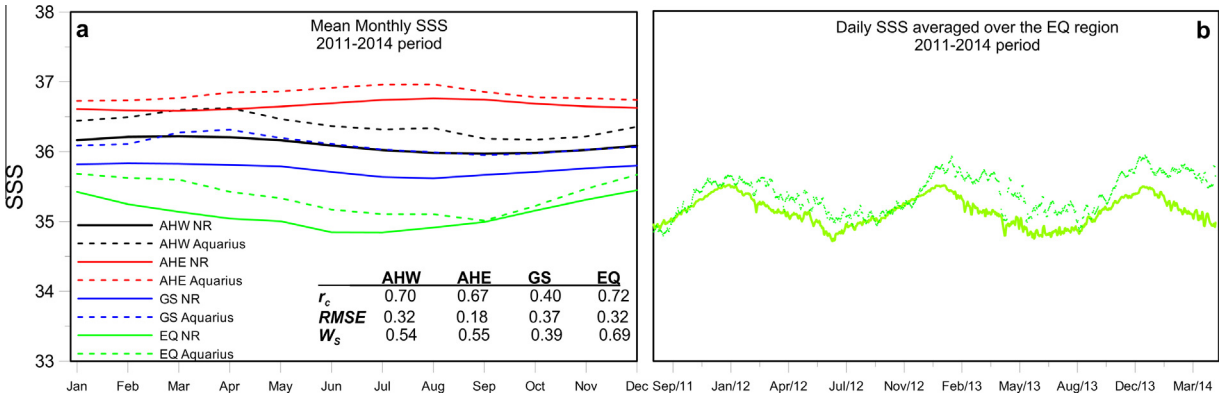

Fig. 6. Sea Surface Salinity (SSS) temporal variation of (a) monthly mean values, averaged over the four ATL-HYCOM 0.04° sub-regions, and (b) daily values, averaged over the EQ area, as derived from 4 years (2011–2014) of daily Aquarius observations (dashed line) and NR simulation (solid line) data. The Pearson Correlation coefficient (r_C), the *RMSE*, and the Willmott skill score (W_s) between the NR simulation and the SSS daily Aquarius observations are also presented.

data over the 2009–2014 period did not contain enough observations for full coverage of the model domain. Therefore, we employed the historical drifter data to compile a climatology that is suitable for NR evaluation. Respective averaged current fields were derived from the 6-year NR simulation and also from AVISO-derived currents (see Section 2.3.3), which do provide full coverage for the same 6-year period.

The major N. Atlantic surface circulation patterns are well simulated by the model (Fig. 7). The North Brazil Current (NBC), south and north of the Amazon Delta, reveals similar mean annual velocity levels between the NR simulation and the GDP long-term data. The NBC transfers significant amounts of water, including freshwater from the Amazon and Orinoco Rivers, northwestward along the coast of northern Brazil, French Guiana, and Suriname. The maximum NBC current velocities, annually averaged, range around 1.1 m/s and 0.9 m/s for the GDP (Fig. 7a) and NR (Fig. 7b), respectively, in agreement with Arnault et al. (1999) and Bourles et al. (1999), who showed that generally the current flows between 0.6 and 1 m/s but may also reveal peak speeds of 1.1 m/s. The connection of the NBC with the eastward North Equatorial Countercurrent (NEC) (Condie, 1991) is also captured by both GDP measurements and NR simulations around 10°N latitude and 50°W longitude; the mean annual eastward velocity levels over this retroflection region are similar between simulation and observations (~0.22 m/s). The remainder of both observed and simulated NBC continues northwestward to join the Guiana Current. The strong Caribbean Current (CC), formed around 15°N, carries warm surface waters westward and inside the Caribbean Sea. Fratantoni (2001) showed that the highest surface velocities may reach 0.7 m/s; the NR simulated annual velocities range around 0.75 m/s (Fig. 7b), while the respective GDP values are a bit stronger and equal to 0.80 m/s (Fig. 7a). It should be noted that the GDP averaging method is based on the methodology by Lumpkin (2003). Fratantoni (2001) did simple bin averaging, which may underestimate peak speeds (as in the Gulf Stream) for two reasons: first, because slower drifters stay in a bin longer and contribute more velocity observations, biasing the value low; and second, because the core will be more heavily smoothed across the bin. Further downstream, the Loop Current and the Florida Current, both parts of the Gulf Stream system, are apparent in both NR and GDP circulation fields. The former enters the Gulf of Mexico with maximum velocity levels around 0.8 m/s and the latter exits along the Florida Strait and toward the North Atlantic Ocean with velocity levels that may reach 1.2 m/s, as described by both drifter measurements and the NR

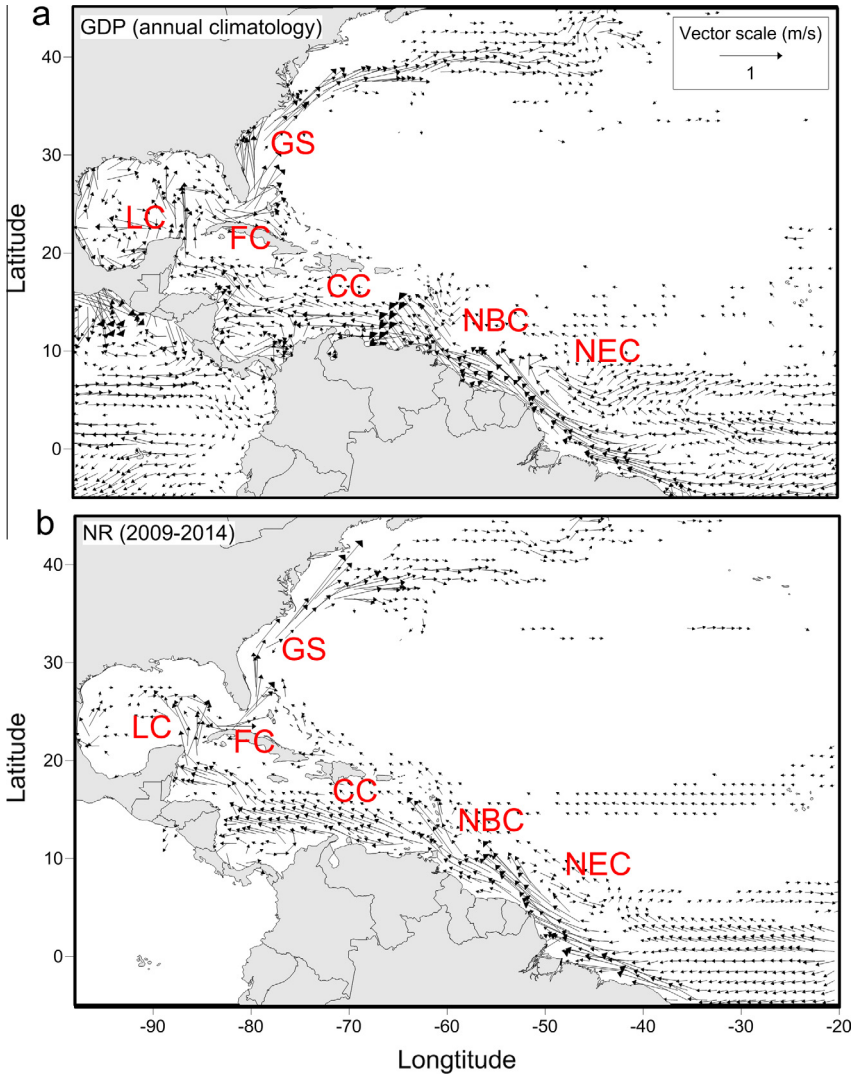

Fig. 7. Mean annual distribution of near-surface currents (m/s) as derived from (a) GDP measurements and (b) NR simulation over the entire model domain (both calculated at 15 m). The Pacific Ocean distribution is excluded from the NR simulations. Velocities lower than 0.1 m/s are not plotted for clarity. Red letters indicate major currents: North Equatorial Countercurrent (NEC), North Brazilian Current (NBC), Caribbean Current (CC), Florida Current (FC), Loop Current (LC), and main Gulf Stream (GS).

simulation and in agreement with Leaman et al. (1987). The Gulf Stream along the eastern U.S. coastline reveals strong surface mean annual velocities that may reach 1.5 m/s. The averaged Gulf Stream position as it leaves the coast, off Cape Hatteras, North Carolina, is the same in both observed and simulated fields (~35°N), in agreement with Halkin and Rossby (1985). An eastward jet, stronger than the Florida Current, is observed around 70°W between 35°N and 40°N and it gradually attenuates as it travels offshore toward the central Atlantic, in both drifter and NR fields.

As mentioned above, the long term drifter climatology was used, due to the limitations of drifter data coverage during 2009–2014. This limitation did not allow derivation of a comprehensive surface circulation field in some sub-regions of the study domain, as is available from the model simulation. We employed the AVISO derived currents (2009–2014) for further evaluation and analyses (Fig. 8). Both comparisons, with current speed at 15 m from GDP (Fig. 8a) and surface geostrophic current speed from AVISO-derived current fields (Fig. 8b), show good agreement, with strong mean velocities (~1.0 m/s) along the Gulf Stream and along the northwestward NBC. The Loop Current intrusion into the Gulf of Mexico is evident in the model and data fields.

The monthly mean Kinetic Energy (KE) from the AVISO-derived surface currents is computed and averaged over the four sub-regions (Fig. 9). The highest KE, with strong seasonal variation, is observed over the EQ area (Fig. 9a) during the summer months. The variations from both model and observations show similar results with strongest currents over the equatorial region. The lowest levels from both model and data occurred over the AHE region, where seasonal variation is absent. The overall coefficient of determination is very high (R^2 = 0.96), as well as the Pearson correlation of the NR-AVISO monthly values (r_c = 0.98), see Fig. 9b. The total linear fit between the simulated and observed monthly values is almost perfect, close to the $y = x$ equation (linear fit: $Y = 0.87X + 0.01$). The averaged simulated and observed values of all sub-regions are almost identical, at 0.057 m^2/s^2 and 0.060 m^2/s^2, respectively. For each separate region, the averaged simulated (first) and observed (second) values are: AHW (0.045, 0.049); AHE (0.014, 0.021); GS (0.063, 0,067); EQ (0.105, 0.102), indicating a satisfactory performance of the model with respect to surface circulation at each sub-region.

3.3. Evaluation of upper ocean structure

The model performance over the upper ocean (100 m) is highly important for the investigation of the hurricane-ocean interactions, since it is a typical depth of vertical mixing by most hurricanes (Price, 2009). Nonlocal processes such as upwelling over the upper ocean and the stratification structure affect the characteristics of hurricanes over the open ocean (Price, 1981). Herein, we use the

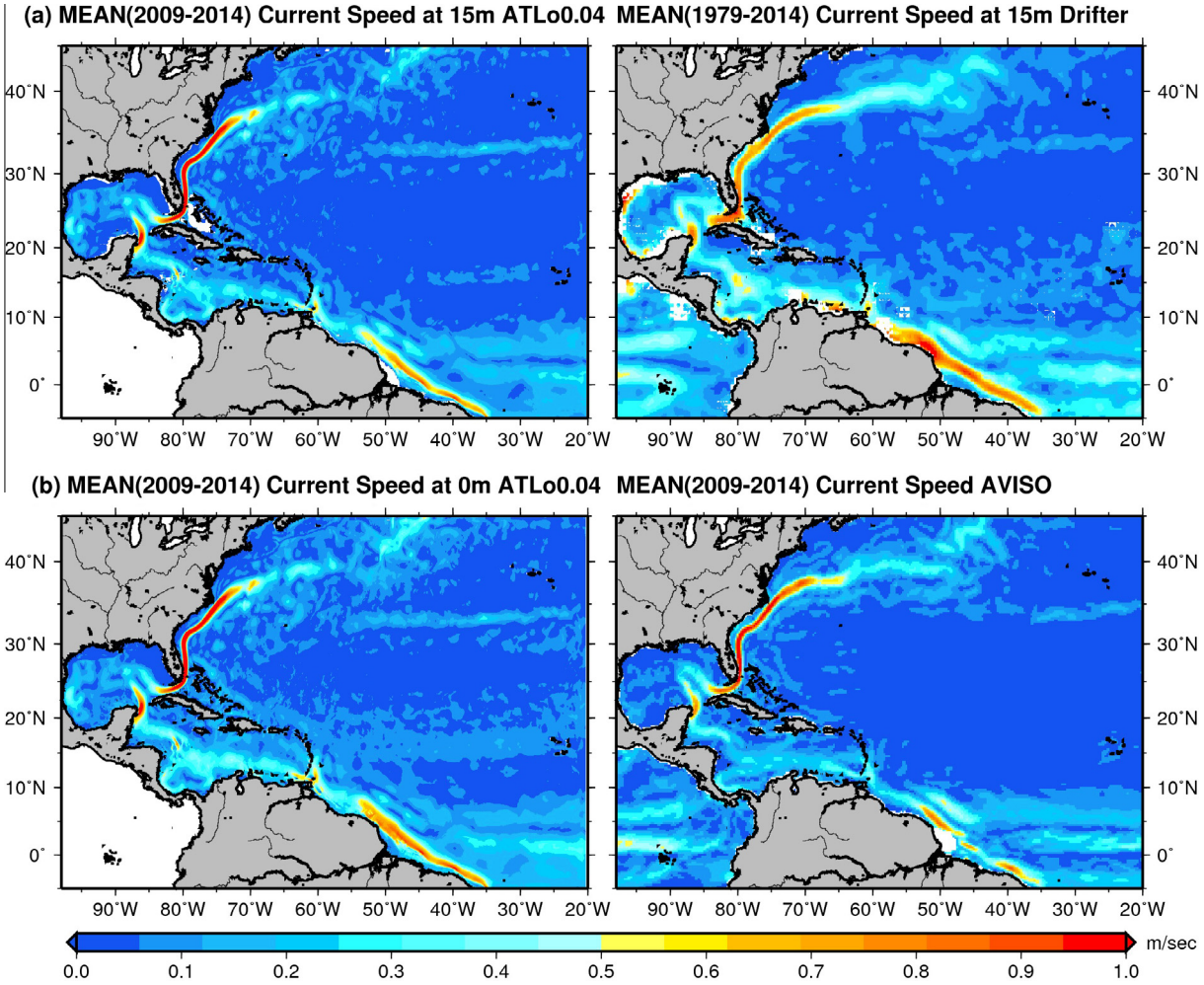

Fig. 8. Mean annual distribution of near-surface currents (m/s) as derived from: (a) NR simulation (2009–2014, left) and GDP measurements at 15 m (1979–2014, right); (b) NR simulation (2009–2014, left) and AVISO observations at the surface (2009–2014, right). The NR currents are extracted to match observational depths at 15 m (GDP) and surface (AVISO). The Pacific Ocean distribution is excluded from the NR simulation.

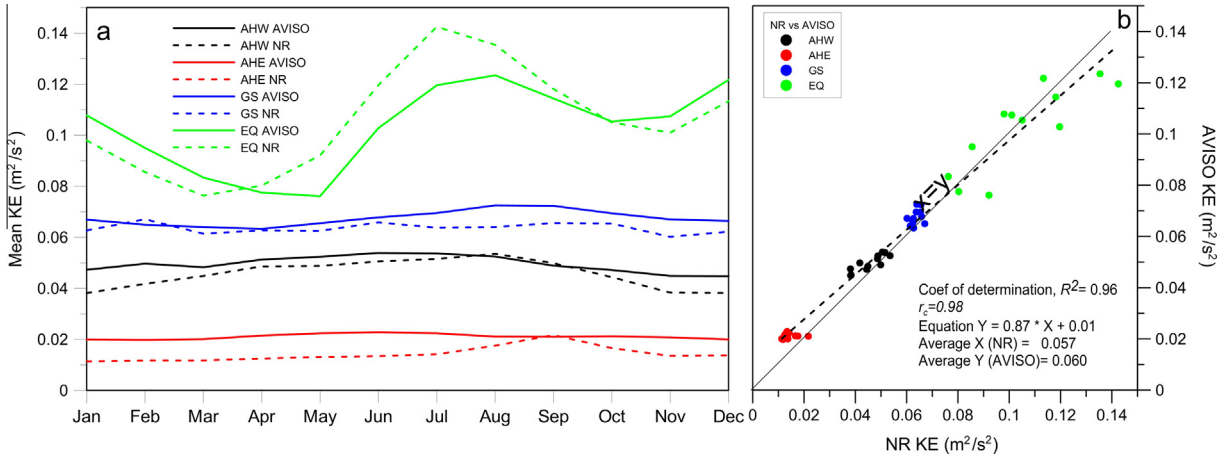

Fig. 9. (a) Monthly evolution and (b) scatter diagram of climatological Kinetic Energy (KE; $m^2\,s^2$), averaged over the 4 sub-regions as derived from the surface current velocities of NR and the respective AVISO derived values. The overall linear equation, the average annual values, the Pearson correlation (r_c), and the coefficient of determination between model and observations are also presented. See Fig. 1 for the definition of model sub-domains. (For interpretation of the references to colour in this figure legend, the reader is referred to the web version of this article.)

upper ocean available measurements from the Argo system over the N. Atlantic Ocean.

3.3.1. Temperature and salinity differences in the upper ocean

The differences between SST and temperature at 100 m (dT(0–100 m)) and between SSS and salinity at 100 m (dS(0–100 m)) are derived from all available Argo floats (Section 2.2.1) over the study domain and are compared with the respective differences derived from the model temperature and salinity data. dT(0–100 m) and dS(0–100 m) are averaged over each sub-region and the monthly evolutions are presented in Fig. 10a and b, respectively. The agreement between the temperature differences over the AHW region is significantly high, with Pearson correlation coefficient and Willmott skill score very close to 1. The seasonal variation of the difference between both depth levels is very large and varies from periods with extensive vertical mixing (winter: dT(0–100 m) = 0.5 °C) to periods with intense stratification (summer: dT(0–100 m) = 6 °C). In addition, the *RMSE* is 0.34 °C, indicating the good performance of the model over the upper 100 m of the water column, which is a typical layer depth of vertical mixing by hurricanes. It is noted that the regions with large number of available Argo measurements during the 6-year study period show the higher correlation with the respective model derived variables. The AHW, AHE and GS regions reveal high scores and are the areas with higher number of Argo floats, compared to the EQ region (see Section 2.2.1; Table 1). The best correlation is observed for the AHW and GS regions, where W_s is almost 1 and the *RMSE* is very low (~0.30 °C). The lowest correlation is computed over the EQ region, possibly due to the small number of available measurements during the study period (only 2.3 floats per day in this region, corresponding to an area normalized count of 10^{-3} km^{-2}; Table 1 and Section 2.2.1). Despite a slight underestimation of the temperature gradient by the NR, the model performance is still satisfactory, as both measurements and simulation data reveal the

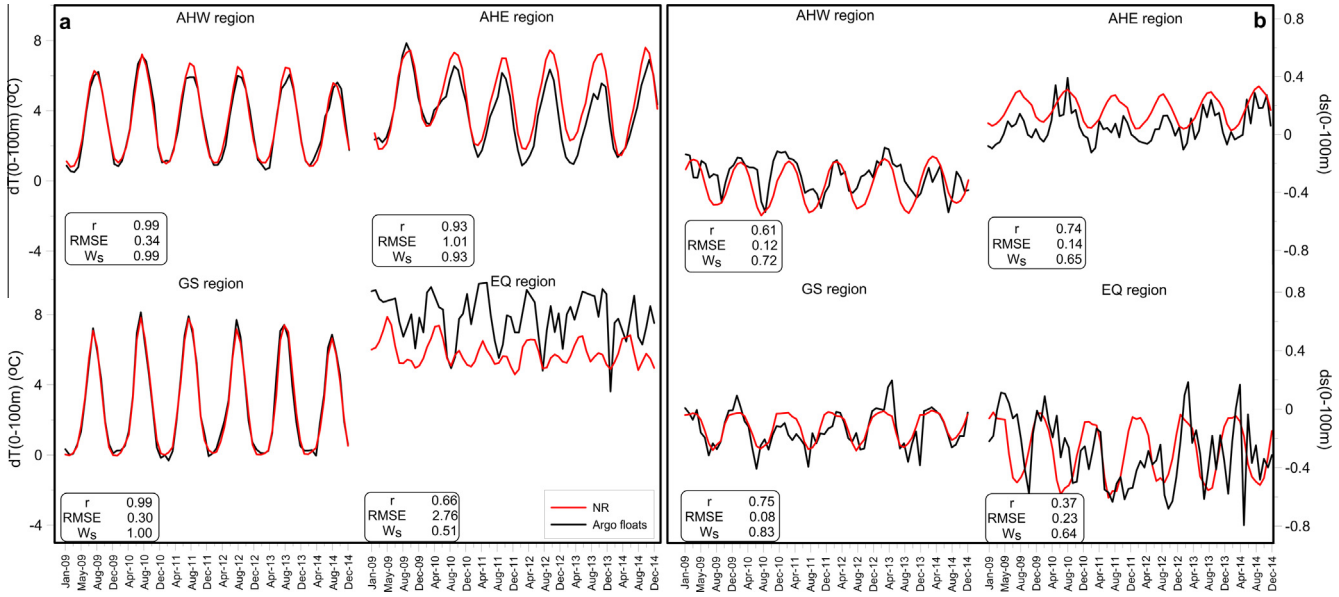

Fig. 10. Monthly evolution of the difference between (a) Sea Surface Temperature (SST) and Temperature at 100 m (dT(0–100 m)) and (b) SSS and salinity at 100 m (dS(0–100 m)), as derived from NR simulation and Argo data over the four N. Atlantic sub-regions for the 2009–2014 period. The respective Pearson Correlation coefficient (r_C), *RMSE*, and Willmott Skill score (W_s) are also presented for each region. See Fig. 1 for the definition of model sub-domains. (For interpretation of the references to colour in this figure legend, the reader is referred to the web version of this article.)

highest levels of *dT*(0–100 m) at the EQ region, due to the stronger equatorial upper ocean stratification; both time series have values above 4 °C and smaller variation range in comparison with the other three sub-regions (Fig. 10a).

Salinity comparisons also show high scores over the AHW and GS regions, with *Ws* around 0.72 and 0.83, and *RMSE* around 0.12 and 0.08, respectively (Fig. 10b). Although the *RMSE* in the EQ region is almost double than in the other regions, it remains in satisfactory range and is equal to 0.23, which is a very low error for salinity comparisons. The Willmott score is equal to 0.64, indicating that a satisfactory performance of the model with respect to the salinity vertical structure also holds in the EQ region. This corroborates the good agreement of SSS model values to the Aquarius data (Fig. 6a) and GDEM climatology (Fig. 2b). In all regions, the simulated *dS*(0–100 m) follows the seasonal variation of the *in situ dS*(0–100 m), with large negative numbers during summer (<−0.4) and values around zero during winter months. The AHE region shows low and positive differences (not exceeding 0.4) between the SSS and salinity at 100 m (Fig. 10b) due to the highest surface salinities that characterize the subtropical gyre in this region (Fig. 2b).

3.3.2. Upper ocean stratification

The stratification frequency (Brunt-Väisälä frequency; *N*) of the upper ocean is also computed in order to investigate the vertical mixing ability of the water masses located between 0 and 100 m:

$$N^2 = \frac{(-g/\rho_o)(\rho_1 - \rho_2)}{\Delta z}$$

where g is the gravitational acceleration (9.806 m/s^2), ρ_o is the initial ambient mean density (1022.4 kg/m^3), ρ_1 and ρ_2 are the upper and lower layer mean density respectively, and Δz is the thickness of each layer in order to calculate the mean stratification frequency of the upper 100 m.

Fig. 11 presents the mean monthly evolution of stratification frequency (*N*) over the upper 100 m, averaged over all regions from the NR simulation and Argo observations for the 2009–2014 study period. Strong seasonal variation is observed for the AHW region; weak stratification (low *N*) is observed during winter months in both simulated and measured data (<0.004 s^{-1}), while the highest *N* values (strong stratification) were calculated during the end of summer and beginning of fall (~0.006 s^{-1}). Both simulated and observed mean monthly values gradually increase from April to August due to the formation of summer stratification. The strongest seasonal variations are noted for the GS region, where the significantly cold winter conditions induce intensive mixing of the upper ocean and decrease the *N* frequency to very low levels (~0.002 s^{-1}). Both simulation and observations support the large range of stratification frequencies over this region, with significantly higher levels during the summer months. Weaker seasonal variation of stratification conditions occur over the mid-ocean AHE region, where simulated and observed frequency values do not show any strong seasonal variability during the entire 2009–2014 period. Although the NR simulation underestimates the stratification of the upper ocean, revealing lower *N* frequencies throughout the annual cycle, both simulated and measured seasonal range is smaller than in the AHW and GS cases. The *N* values derived from the Argo floats in the EQ region show a non-seasonal, irregular variation, possibly due to the low number of available Argo measurements (Table 1). The NR results show a clear seasonal variation, revealing strongest stratification conditions in July due to the warm and rainy summer conditions over the equatorial region. The inter-annual comparisons between the Argo and NR time series (not shown) also revealed better model performance for the AHW and GS regions, with higher *N* values during all summers and lower levels during all winters, when vertical mixing is stronger.

4. Nature Run application: hurricane and ocean interaction over the Gulf Stream extension

In addition to serving as the Nature Run (NR) within the OSSE framework, the data evaluated free-running ATL-HYCOM 0.04° simulation is valuable for several applications, especially the understanding of processes that are often limited by observational gaps. We present such an application of the simulation that was

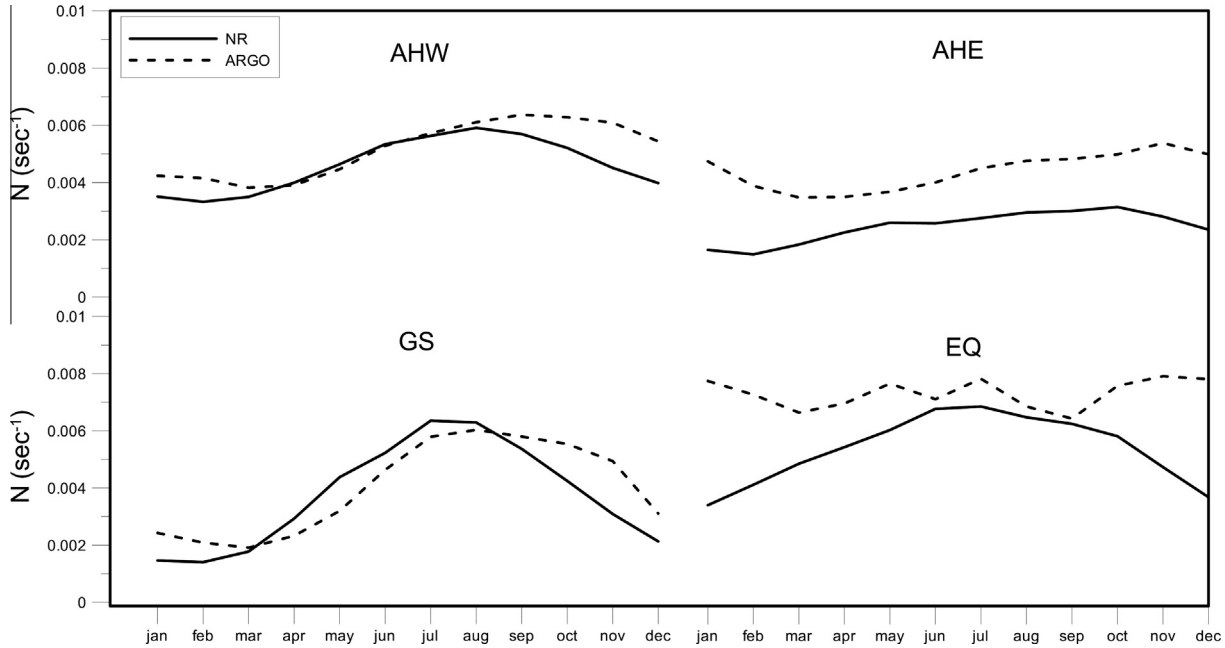

Fig. 11. Evolution of climatological (2009–2014) mean monthly stratification frequency (*N*) averaged over the upper 100 m, and the AHW, AHE, GS and EQ regions from NR simulation (solid line) and Argo observations (dashed line). See Fig. 1 for the definition of model sub-domains.

evaluated in the previous section, focusing on a hurricane related process. We examine the interaction between a major hurricane and a western boundary current, namely the Gulf Stream.

The Gulf Stream flows along the eastern U.S. coasts northward, after its exit from the Gulf of Mexico through the Florida Straits, carrying warmer Caribbean Sea waters toward the North Atlantic Ocean. The northward pathway of the current turns eastward around Cape Hatteras at ~35°N (Figs. 2, 7, and 8), separating away from the coast into deep waters (Halkin and Rossby, 1985); this is the so-called "Gulf Stream extension" area. The eastward Gulf Stream transport between 35°N and 40°N is approximately twice as large as that observed in the Florida Straits (Knauss, 1969; Johns et al., 1995). The Gulf Stream position as it leaves the coast varies throughout the year (Auer, 1987; Kelly and Gille, 1990; Frankignoul et al., 2001). At the end of summer and especially during fall, the current transports the maximum amount of water (Kelly and Gille, 1990). A hurricane event that reached the Gulf Stream extension area during 2009 (Hurricane Bill, HB) is examined during the process oriented study. We focus on the upper ocean response and the Gulf Stream evolution during the hurricane passage, defined by the HB core passing over the main Gulf Stream front. We employ the AHNW and extended AHNW sub-regions (Fig. 1), where the main interaction between the Gulf Stream and HB took place.

The HB track and intensity every 6 h during August 2014 was obtained from the National Hurricane Center (http://www.nhc.noaa.gov) "best track" archives. We focus on the location of the hurricane "eye", investigating its interaction with the Gulf Stream over the northwestern area of the study domain in August 2009 (see Section 4.1). However, we note that the hurricane interaction with the ocean waters covers a much broader area.

4.1. Hurricane Bill evolution and ocean interaction

The 2009 Atlantic season was marked by below-average TC activity. However, HB affected the eastern U.S. and Canadian coasts by producing high surf, rip currents, and beach erosion (Berg and Avila, 2010). The coverage of the entire hurricane and Gulf Stream evolution regions by the ATL-HYCOM 0.04° domain and the good performance of the simulation, especially over the upper 100 m (Section 3.1), consist a useful and efficient simulation platform for the investigation of the upper ocean response to hurricane activity.

Fig. 12 presents the HB location at characteristic dates of August 2009, over SST maps. These maps are from the free-running NR, the data assimilative, real-time global HYCOM model and data (available as daily averages) from GHRSST (Section 2.3.1). The global HYCOM output is included in this comparison, to represent realistic ocean conditions from a robust operational forecast system. Its output is daily available at 00:00 GMT and, therefore, we have also chosen to present the respective 00:00 GMT archives from the NR simulation in Fig. 12 for comparison. HB was formed over the AHE region on 15 August, 2009 and was upgraded to Category 4 (<955 hPa) intensity around 20 August over the central AHW region (Fig. 12a). HB slightly weakened (Category 3) before its entry into the AHNW region on 22 August (Fig. 12b), where it transitioned to extratropical status. The HB interaction with warmer waters began on 21 August and the storm passed over the AHNW region on 22 and 23 August (Fig. 12c). It finally reached the eastern Canadian coasts on 24 August, downgraded to a Category 2 hurricane (>963 hPa) and completely dissipated on 27 August 2009. HB reached the Gulf Stream extension over the AHNW region after covering a distance of 4,700 km. The SST from the free-running NR is in good agreement with both data assimilative model and satellite observations. The hurricane track in relation to the cold wake formation simulated by the model is also in agreement with the track documented by the National Hurricane Center (Avila, 2010). The expected influence of the hurricane to the ocean waters is the strong cold wake along the hurricane track (Fisher, 1958). This effect can be seen in the free-running NR, in agreement with GHRSST data and the global HYCOM re-analysis. This indicates that the NR correctly captures the surface ocean response to the storm influence. The cold wake refers to the intensive SST cooling due to turbulent entrainment driven by shear at the mixed layer base and the upwelling of cooler deep waters (D'Asaro et al., 2007). The difference between the cold wake's SST and the surrounding waters varied from ~2 °C over the AHW region (Fig. 12a) to ~7 °C over the AHNW region (Fig. 12c), where the pre-existing and surrounding surface layers were largely affected by the warm Gulf Stream extension.

The HB interaction with the warmer surface waters intensified the storm, in agreement with a process described by Nguyen and Molinari (2012) during Hurricane Ivan. These rapid intensification events are particularly challenging to predict, and they are often missed by operational forecasts (Elsberry et al., 2007). The high oceanic heat content is one of the factors that have been often associated with rapid intensification (Shay et al., 2000; Kaplan et al., 2010). Here, we use the three-dimensional NR fields to investigate a feedback from the hurricane to the warm western boundary current.

4.2. Upper ocean response to the hurricane passage

Fig. 13 presents time series of hurricane related parameters to better describe both the HB evolution and the upper ocean response. Wind speed within the hurricane (Fig. 13a) increased and pressure decreased (Fig. 13b) until ~mid-August (Avila, 2010). HB slightly weakened on 20 August around noon, but its winds strengthened and its pressure dropped again on 21 August; by midnight it had reached its lowest pressure of 943 mb. A clear SST increase is observed (GHRSST) and simulated (NR) over the AHNW region during the first 20 days of August (Fig. 13c). This is due to an overall increase in the SST within the western part of the North Atlantic subtropical gyre and to the extension of the Gulf Stream front within the AHNW region. The cold wake of HB reduced the SST in the AHNW region (Fig. 13c) and increased the Mixed Layer Depth (*MLD*) from 10 m to 30 m on 23 August (Fig. 13d), when the hurricane's core was in the northern part of the study sub-region (Fig. 12c). The stratified upper ocean associated with the Gulf Stream in the AHNW region became mixed under the HB effect, and the stratification frequency N_{AHNW} showed a rapid reduction, reaching its lowest levels on 23 August, as derived from both NR simulations and Argo floats measurements (Fig. 13e). Both *MLD* increase and N_{AHNW} reduction occurred simultaneously with the appearance of the HB core over the AHNW region and the SST reduction over the storm's cold wake. The short intensification of the storm on 21 August was interrupted after the collapse of the upper ocean stratification and the limitation of the Gulf Stream eastward spreading; a sharp wind speed decrease and SLP increase were marked during the HB passage over the AHNW region on 22 and 23 August (Fig. 13a and b). We deduce that the eastward flow of the Gulf Stream was directly impacted by the hurricane passage, an important effect of atmospheric influence on the evolution of a western boundary current.

We first examine if these effects were unique to HB, or if they are similar to the influence that other hurricanes had on the upper ocean structure in the study region. Fig. 14 shows the evolution of all hurricanes (13 total) that crossed over the extended AHNW region (Fig. 1) during the 2009–2014 period. The measured (National Hurricane Center data) minimum pressure in the "eye" of each hurricane (Minimum Central Pressure, *MCP* in hPa) is given. In all 13 cases, *MLD* increases when the hurricanes passes over the

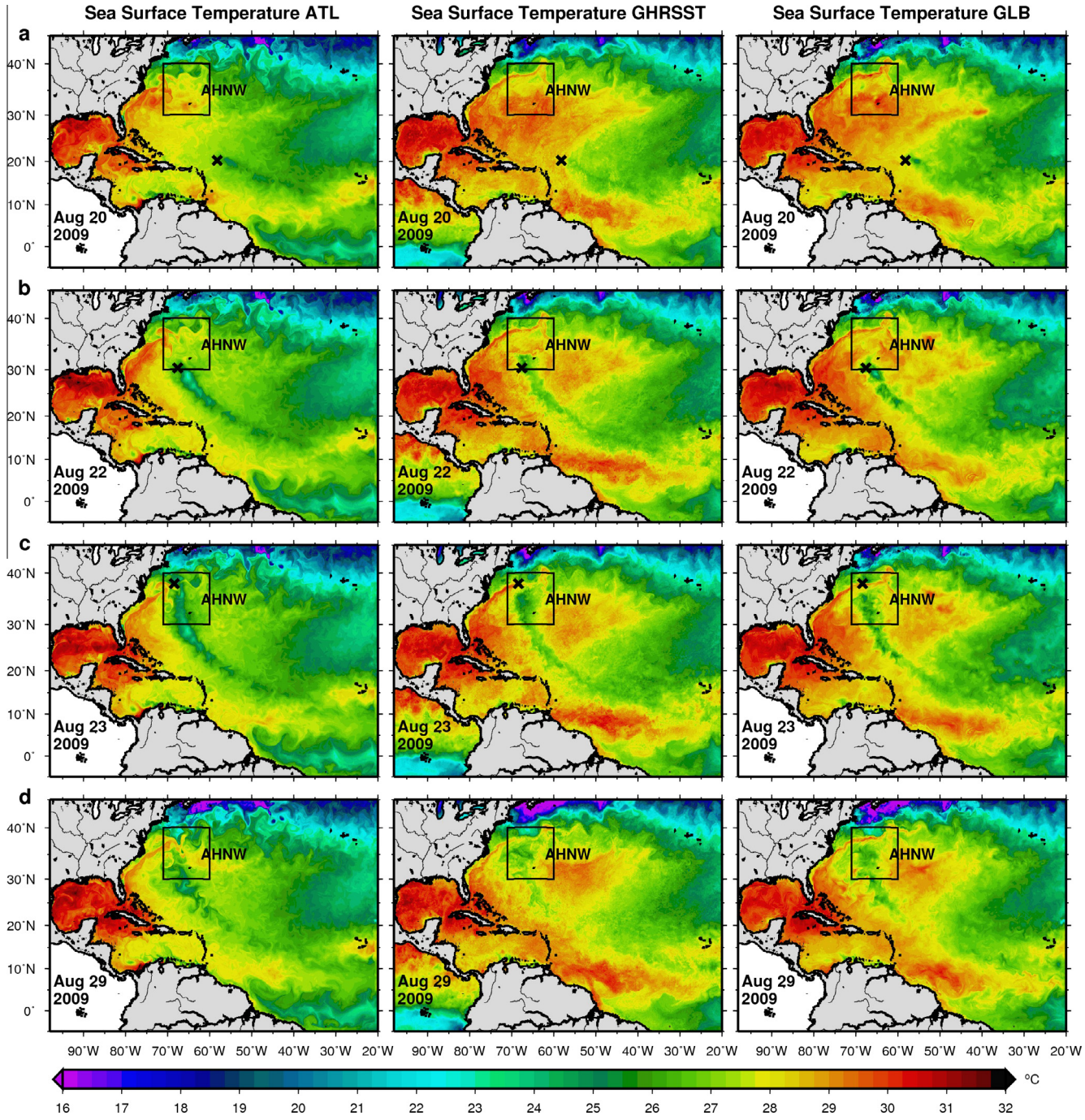

Fig. 12. Distribution of Sea Surface Temperature (SST) on (a) 20 August 2009, (b) 22 August 2009, (c) 23 August 2009 and (d) 29 August 2009, derived from the NR (ATL-HYCOM 0.04°) simulation (left), GHRSST data (middle) and global (GLB-HYCOM) simulation (right). The position (x) of Hurricane Bill along the cold wake signal (at 00:00 GMT) and the AHNW region are also indicated. (For interpretation of the references to colour in this figure legend, the reader is referred to the web version of this article.)

AHNW region. *N* stratification reductions are also observed during all hurricanes, especially during summer months, when pre-existent stratification is stronger (e.g. Hurricanes Bill, Bertha and Cristobal). The hurricane effects on upper ocean stratification and *MLD* are moderate during October (e.g. Hurricanes Rafael, Fay and Gonzalo), when the stratification frequency has already decreased, as part of its seasonal cycle, and the respective *MLD* is usually larger than in summer. However, stratification frequency and *MLD* reached their lowest ($\sim$0.01 s^{-1}) and highest ($\sim$70 m) levels between all 2009–2014 cases during Hurricane Sandy, which was a severe storm that propagated along the Eastern U.S. coasts and interacted with the GS extension region (Galarneau et al., 2013).

The horizontal transport, integrated over the upper 100 m across the 35°N–38°N section at 70°W, is presented in Fig. 15. Fig. 12 showed that the Gulf Stream eastward extension was evident across this latitudinal section during the HB evolution over the northwestern Atlantic. A substantial transport decrease of approximately 5 Sv occurred during the HB passage over the area, when its cold wake was fully developed in the western side of the study section (Fig. 12c). This result indicates that the storm impact reduced the eastward transport along this main Gulf Stream extension pathway over the N. Atlantic Ocean. Finally, a strong eastward advection of upper ocean waters ($\sim$18 Sv), was noted at the end of August (Fig. 15), indicating the recovery of the Gulf Stream east-

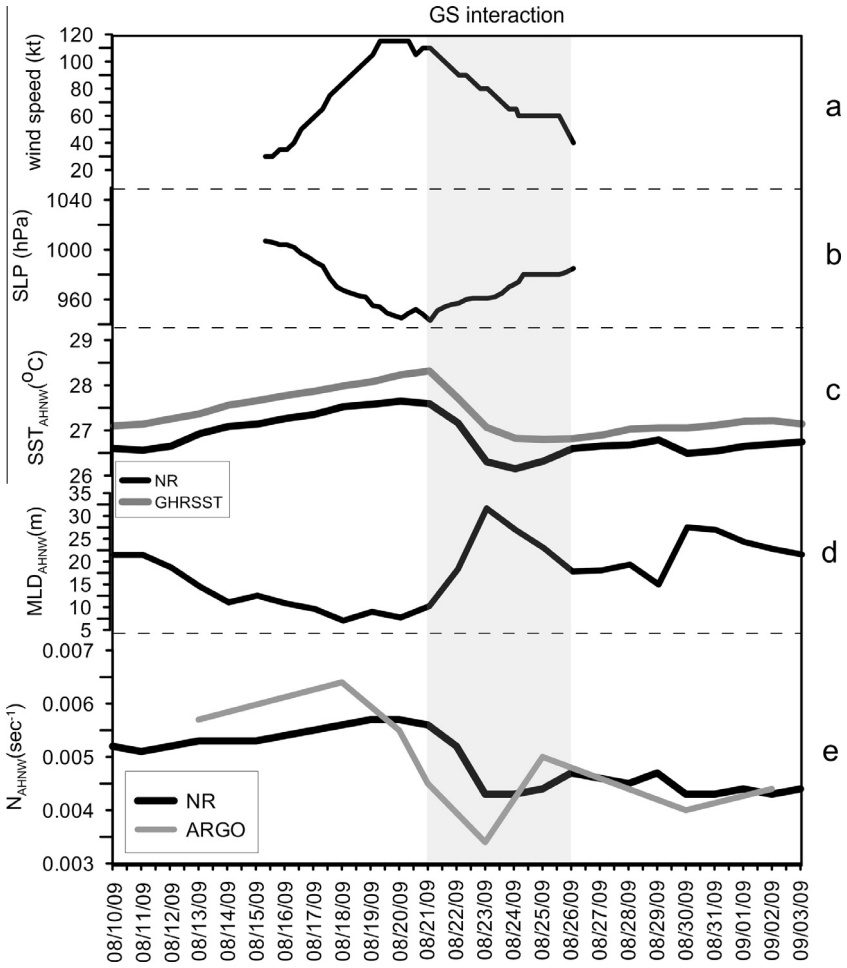

Fig. 13. Evolution of (a) wind speed (kt) and (b) 6-hourly Sea Level Pressure (SLP, hPa) of Hurricane Bill (based on National Hurricane Center data). Evolution of daily (c) Sea Surface Temperature (SST_{AHNW}, °C) from the NR simulation (black) and the GHRSST data (gray), averaged over the AHNW region. (d) Evolution of Mixed Layer Depth (MLD_{AHNW}, m), averaged over the AHNW region from the NR simulation. (e) Evolution of daily stratification frequency N_{AHNW} (s^{-1}), averaged over the upper 100 m and the AHNW region from the NR simulation (black) and the available Argo floats (gray). All temporal evolutions refer to August and September months of 2009. The period of the hurricane's interaction with the Gulf Stream extension is indicated with a gray shaded area.

ward extension after the northward propagation of the storm and its final dissipation.

Fig. 16 presents more details on the variability of currents and SST, which is dominated by the interaction between the Gulf Stream and the hurricane induced circulation and cold wake, over the AHNW region. The GHRSST derived distribution of SST is also presented for a more detailed comparison with the NR fields. Examination of the entire North Atlantic current field during the hurricane passage (Fig. 16a and b) reveals that the cold wake is marked by a meandering circulation. The successive positions of the hurricane core create cells representing the near-inertial wave wake forced by the storm, which consists of alternating anticyclonic and cyclonic cells; the latter favor the upwelling of deep, cold waters. As seen in Fig. 16c, the Gulf Stream eastward jet is confined between 37°N and 38°N on 22 August, when the HB core is located over the southern part of the AHNW region. Both the NR and GHRSST fields show that the larger part of the region is covered with warm waters (>28 °C), while the HB cold wake is still located to the south of the Gulf Stream. The HB intrusion reduced SST and formed a westward cyclonic turning of the surface waters, over the southwestern AHNW area. As the HB core traveled over the Gulf Stream front on 23 August (Fig. 16d), it created an intense current field, characterized by circulation cells south and north of the Gulf Stream main flow. These cells influenced the eastward flowing Gulf Stream. The southern cell created a southwestward turning, while the northern cell created a northwestward turning. This diversion was localized in the area of interaction between the cold wake and the warm Gulf Stream waters, influencing the Gulf Stream extension, as also evident in the SST fields (both from the NR, global HYCOM and GHRSST data, Fig. 12). The passage of HB thus diverted and weakened the Gulf Stream eastward flow in agreement with the transport drop presented in Fig. 15. The Gulf Stream front was drastically restricted until the hurricane exit from the domain (August 24, Fig. 16e), recovering after several days (August 30; Fig. 16f), when the cold wake was also significantly reduced. Warmer waters (>28 °C) began to spread again toward the East, indicating the recovery of the Gulf Stream eastward pathway after the HB passage and the strong transport increase (Fig. 15). The cold wake attenuation south of 37°N is also observed in the GHRSST measurements (Fig. 16f). Further evidence of the current evolution is given in Fig. 16g, through the trajectory of a single drifter that went through AHNW during and especially after the HB passage. Strongest drifter speeds (2–2.5 m/s) were measured during 26–28 August, after its entrance in the AHNW region and with an eastward path along the high velocities of the Gulf Stream extension. This indicated the eastward flow recovery of the Gulf Stream after the HB passage, in agreement with the transport increase presented in Fig. 15. It is noted that the overall drifter trajectory inside the AHNW region was determined by the anti-clockwise circulation of the storm's cold wake following the

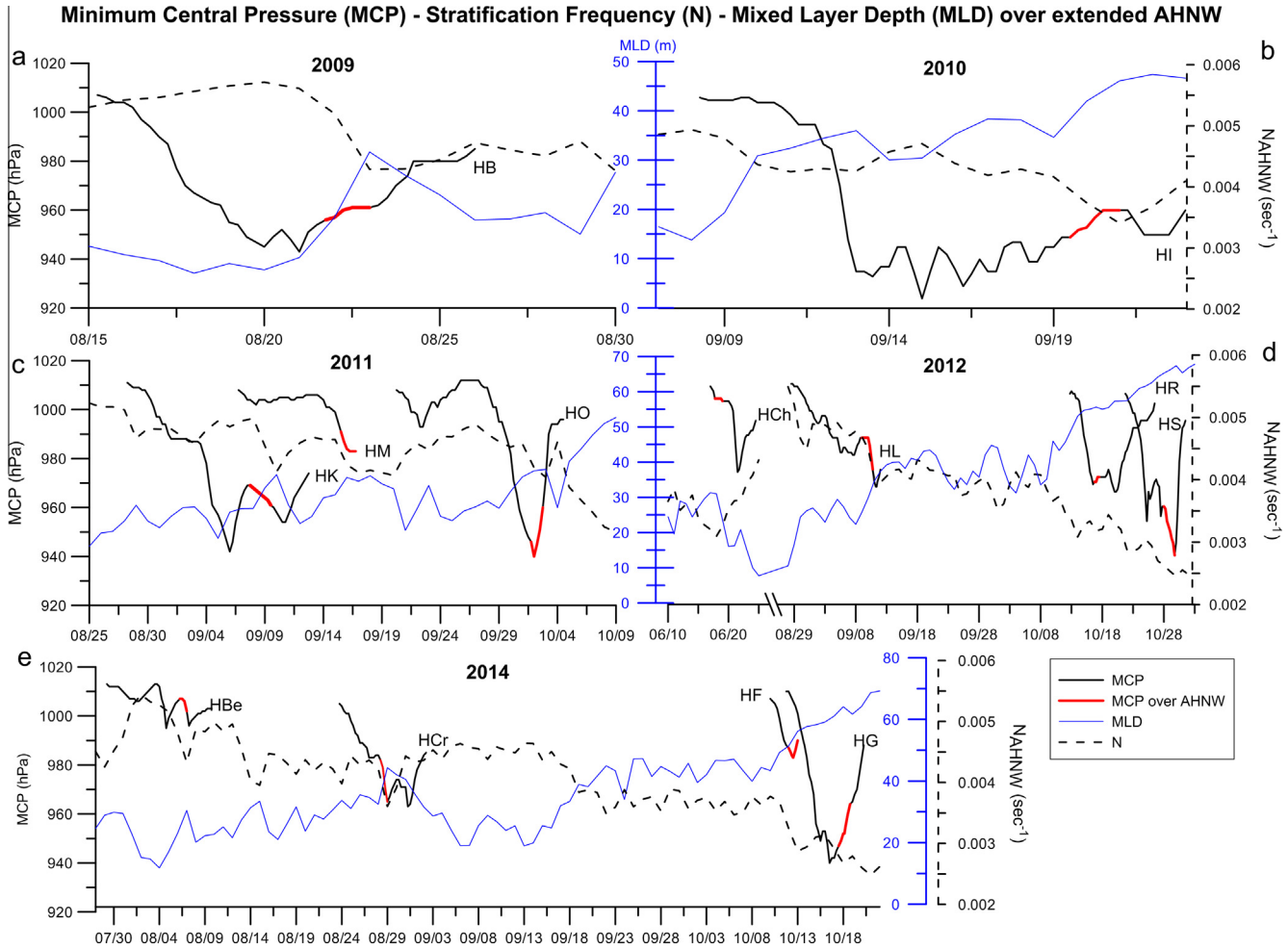

Fig. 14. Evolution of all hurricanes (tropical storms and depressions are excluded) that crossed over the extended AHNW region (Fig. 1) during the 2009–2014 period. Measured (National Hurricane Center data) Minimum Central Pressure (*MCP*, in HPa, black line), simulated Mixed Layer Depth (*MLD*, m; blue line), and simulated *N* stratification frequency (s^{-1}, dashed line) over the upper 100 m and averaged over the AHNW region are presented. Red color indicates the passage of each hurricane over the AHNW region. Hurricanes (a) Bill (HB), 2009; (b) Igor (HI), 2010; (c) Katia (HK), Maria (HM), Ophelia (HO), 2011; (d) Chris (HCh), Leslie (HL), Rafael (HR), Sandy (HS), 2012; (e) Bertha (HBe), Cristobal (HCr), Fay (HF), Gonzalo (HG), 2014 are presented. No hurricanes were observed over the AHNW region in 2013. (For interpretation of the references to colour in this figure legend, the reader is referred to the web version of this article.)

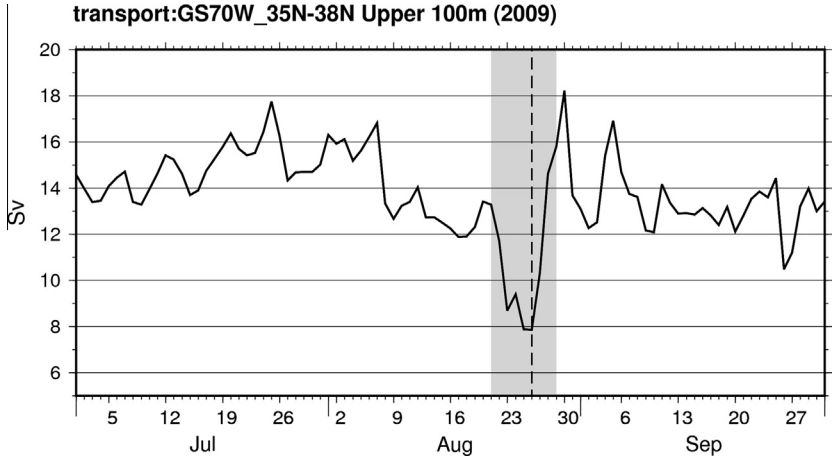

Fig. 15. Daily evolution of transport (Sv) across the 35°N–38°N section at 70°W for the upper ocean (0–100 m) from July to September 2009. The shaded area indicates the passage of Hurricane Bill core over the Gulf Stream extension. The vertical dashed line marks 26 August, when the hurricane core started leaving the Gulf Stream extension region.

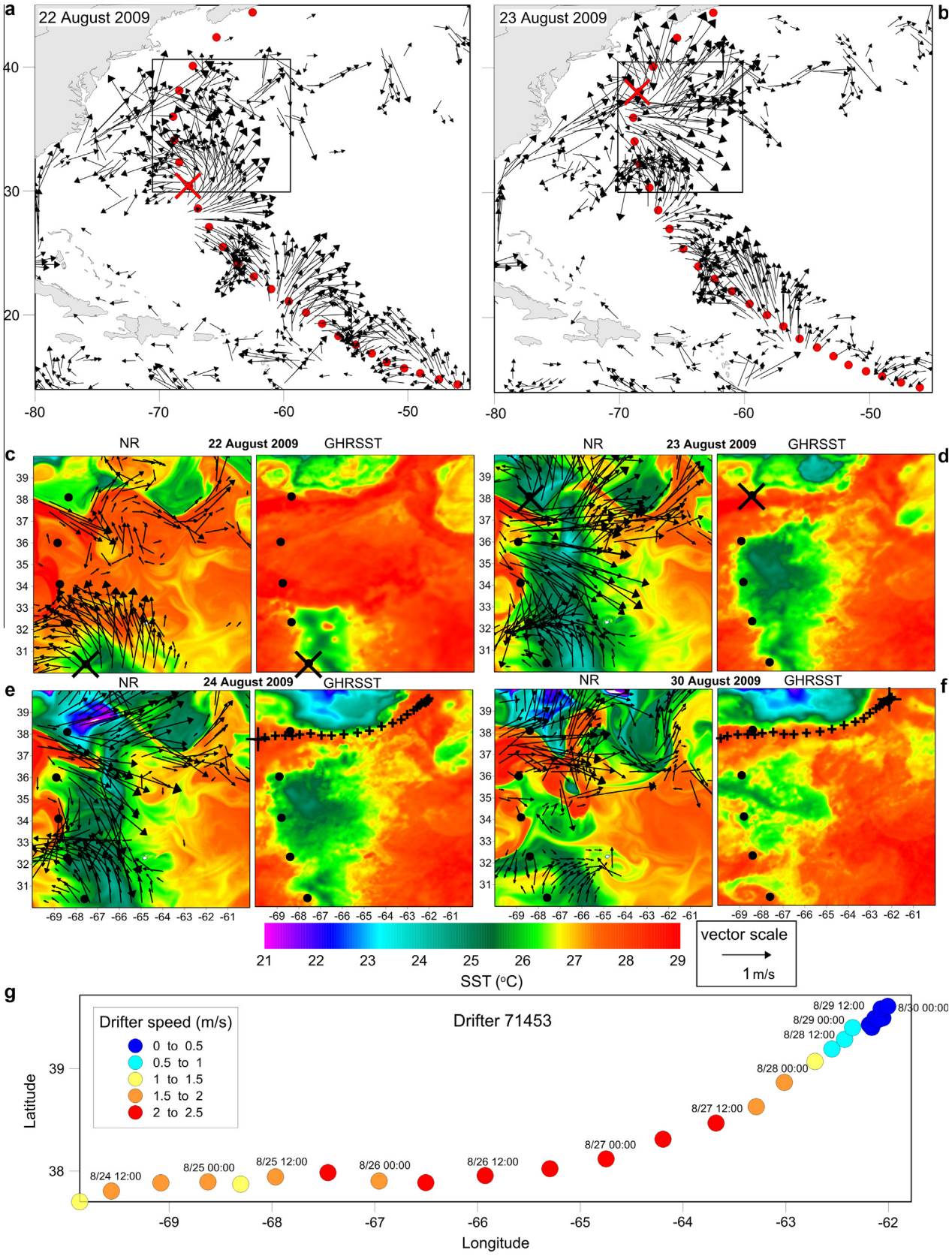

Fig. 16. (Upper): Circulation along the Hurricane Bill (HB) path on (a) 22 August and (b) 23 August 2009. (Middle): Distribution of surface current velocities (m/s) and SST (°C) over the AHNW region on (c) 22, (d) 23, (e) 24, and (f) 30 August 2009 (dates above each panel pair) as derived by the NR simulation (left panels) and GHRSST observations (right panels); only vectors larger than 0.5 m/s are plotted. The location of the HB track and core (every 6 h) are indicated with black (in lower plots) and red (in upper plots) dots and "x" symbol, respectively. (Lower): Trajectory of drifter #71453 through AHNW during 24–30 August (dates marked on each drifter position); circle colors denote drifter speed (in m/s, values in the box insert). The trajectory is also marked on the GHRSTT panels for 24 and 30 August, with small "+" symbols (every 6 h); the large "+" symbols denote the initial and final drifter position within AHNW. (For interpretation of the references to colour in this figure legend, the reader is referred to the web version of this article.)

front between the cyclonic cold eddy and the Gulf Stream eastward flow of warmer waters (Fig. 16e and f).

The upwelling of colder waters along the HB track is also verified by the temperature and vertical velocity distribution, averaged over the upper ocean (80 m). As seen in Fig. 17a, strong upward ocean velocities (positive values) occurred after the storm passage and along its northward propagation. The vertical velocity distribution before the HB passage is characterized by values close to zero, indicating very weak vertical advection. Positive integrated velocities are particularly high in an area between 25°N to 30°N (southern AHNW limit) on 21 and 22 August, when HB significantly intensified (very low *MCP* values, Fig. 14a). The strong upward velocities were maintained over the study region for several days after the storm's exit. The velocity peak is also evident over the entire upper ocean water column during these days, with very strong upward velocities at 70 m depth (>1500 cm/day; Fig. 17b). This resulted in the upwelling of colder waters (Fig. 17c), which is evident from the upper ocean temperature evolution at the location where the HB minimum *MCP* value occurred (24.1°N and 63.7°W). The upwelling period started from the *MCP* minimum on 21 August and continued through approximately 29 August, with upward velocities still evident several days later (4 September; Fig. 17a). The high temperature waters (>28 °C) that covered the upper 50 m before the HB passage were mixed with colder waters from deeper layers, reducing the stratification frequency and temperature of the upper ocean.

4.3. Gulf Stream surface front displacement

We employ the surface and sub-surface manifestations of the Gulf Stream front to study the influence of HB on front displacement. The surface front of the Gulf Stream is defined by the location of the 28 °C isotherm at the surface. The evolution of this isotherm over the study region before and during the HB event revealed significant variability and, therefore, we found it adequate to describe the surface front evolution. For the sub-surface front we chose the location of the 20 °C isotherm at 100 m. Fuglister and Voorhis (1965) defined the sub-surface front to be the location of the 15 °C isotherm at 200 m. However, according to Horton (1984), this particular definition is not unique, and other isotherms at different depths may be used. We tested several isotherms at various depths in order to detect the sub-surface signature of the Gulf Stream during the study period and region and we chose the 20 °C isotherm at 100 m. The depth of 100 m was the deepest where the Gulf Stream signal showed similar extension and coverage to its surface signal during days without significant forcing from the atmosphere (e.g. 20 August 2009; Fig. 18).

The interaction between HB and the Gulf Stream over the extended AHNW region (60°W–80°W, 30°N–40°N; Fig. 1) led to a substantial reduction of the Gulf Stream eastward extension, corroborating the transport patterns discussed in the previous sections. As seen in Fig. 16, the main path of the Gulf Stream surface thermal front varied during the storm's passage over the region. Both surface and sub-surface fronts showed similar evolution and extension before the HB intrusion (20 August 2009), covering almost the entire AHNW region. The propagation of HB beyond 30°N on 22 August induced the withdrawal of the larger part of the surface front west of 70°W; a thin Gulf Stream branch at 37°N remained east of 70°W. These changes are also revealed in the transport calculation along 70°W (Fig. 15). On the other hand, the distribution of the sub-surface front (20 °C isotherm; red line in Fig. 18) did not reveal any significant change under these extreme meteorological conditions. The displacement of the surface front is even larger on 23 August, when all Gulf Stream waters were restricted west of 70°W. Although the HB eye was located over the core of the current on 23 August, the sub-surface thermal front still extended over the entire sub-region. The storm passage thus increased the horizontal separation between the surface and sub-surface Gulf Stream fronts, in agreement with Horton (1984). Hansen and Maul (1970) showed that both the mean and the variance of the separation between the surface and sub-surface Gulf Stream are greater in regions of anticyclonic curvature. In agreement with their findings, the southward turning of the Gulf Stream extension due to the hurricane (23 August, Fig. 16), which

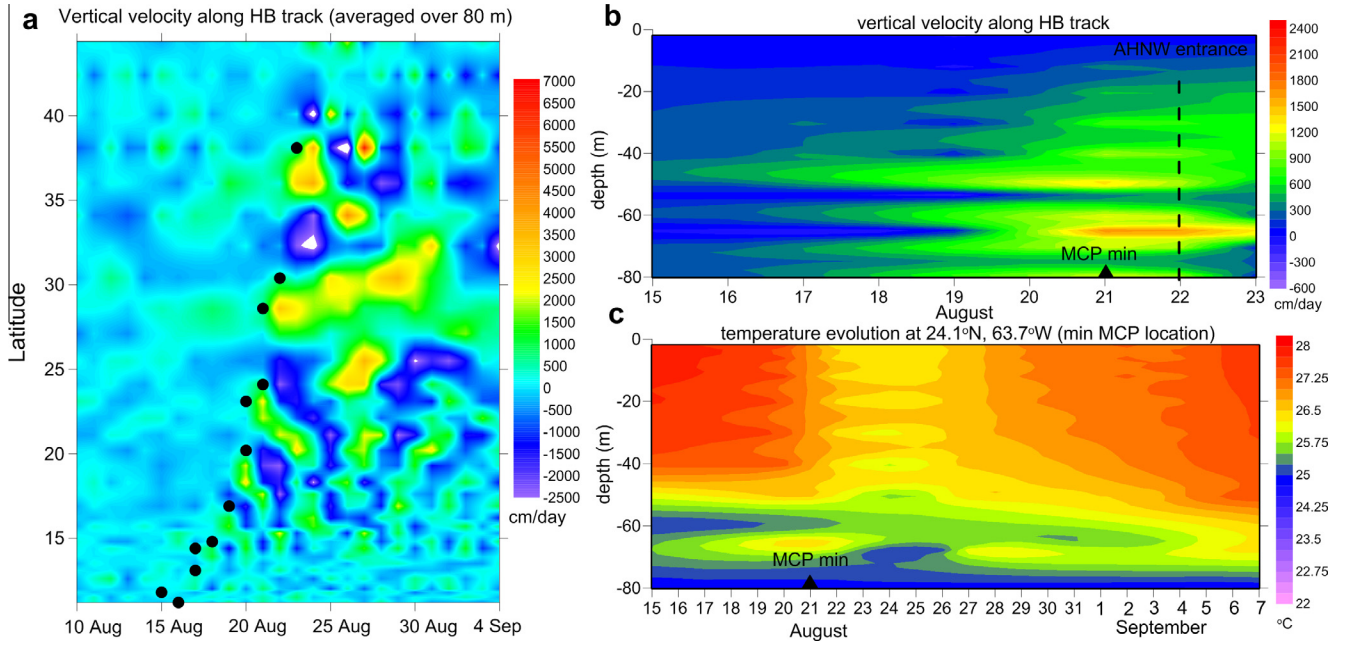

Fig. 17. Hovmöller diagrams of upper ocean (integrated over the upper 80 m) for: (a) vertical velocity along the Hurricane Bill (HB) track from 10 August to 4 September 2009; (b) vertical velocity evolution at each HB "eye" location during the HB passage through the model domain; and (c) temperature evolution at the location where the minimum value for the Minimum Central Pressure (*MCP*) of HB occurred (24.1°N and 63.7°W). The daily track of HB "eye" (black dots in a), the date of HB entrance into the AHNW region (dashed line in b) and the date of minimum *MCP* value (black triangle in b and c) are marked.

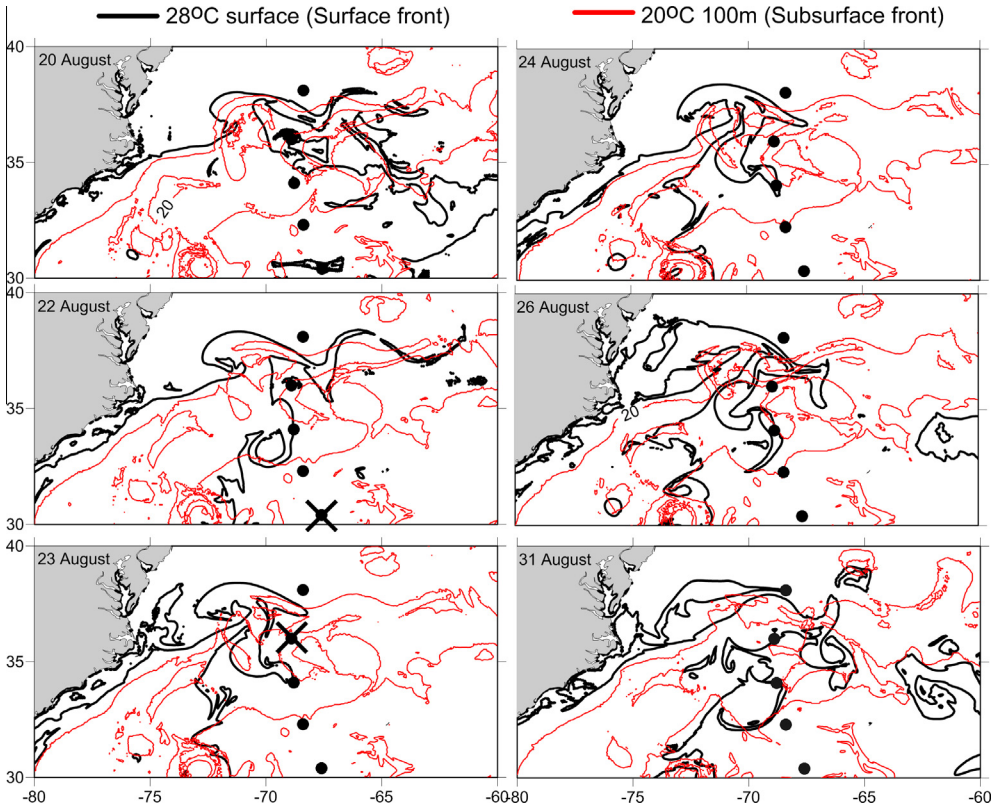

Fig. 18. Plots of surface (28 °C, black lines) and subsurface (20 °C at 100 m, red lines) Gulf Stream fronts over the extended AHNW region (Fig. 1) on 20, 22, 23, 24, 26, 31 August 2009. The Hurricane Bill (HB) track and the exact location of the HB core at each date are indicated with red circles (every 6 h at the hurricane core) and an "x" symbol, respectively. (For interpretation of the references to colour in this figure legend, the reader is referred to the web version of this article.)

enhances the anticyclonic surface currents presented in Fig. 16d and e, is the cause for the large horizontal separation of surface and sub-surface fronts on 23 and 24 August (Fig. 18). The northward HB propagation and the gradual attenuation of its cold wake allowed the eastward spreading of the surface front beyond 66°W by the end of August (31 August, Fig. 18). The sub-surface front did not show any changes during the entire study period. The interaction between the hurricane passage and the evolution of the Gulf Stream front is an important result, expanding our knowledge of the complex interactions between ocean and atmosphere during extreme events. We explore specific components of the ocean response in the next section.

4.4. Diagnosis of geostrophic and ageostrophic ocean circulation

The ageostrophic surface ocean circulation includes the near-inertial wave wake, which can be forced by hurricanes (Shay et al., 1998; Jaimes and Shay, 2010). However, the interactions between forced near-inertial motions and the geostrophic flow field are still not fully understood during hurricane passages (Jaimes and Shay, 2010). The near-inertial response (V_a) is described by the removal of the geostrophic currents (V_g) from the total surface velocities, computed by the model at each model grid point ($V_{total} = V_a + V_g$). The surface geostrophic circulation is computed based on the SSH values from the NR simulation. The u and v components of the geostrophic velocity (V_g), are computed as:

$$fv = g\frac{DH}{DX}$$

$$fu = -g\frac{DH}{DY}$$

where $f = 2\Omega \sin\varphi$ is the Coriolis parameter, with Ω the earth rotation angular velocity and φ the latitude of each cell; DX and DY are the zonal and meridional distances between two successive model grid points where the SSH is computed (DH is the SSH difference between two successive grid points).

Fig. 19 presents the horizontal distribution of Kinetic Energy (KE) derived from surface geostrophic, ageostrophic and total velocities (m/s), summed up over the extended AHNW region (Fig. 1) on 22, 23, 24, August 2009. Note that the ageostrophic currents in the area tend to be more intense than the geostrophic currents, in particular during the passage of HB. This leads to higher levels of KE. However, ageostrophic currents are usually confined in the ocean upper layers, and as such their strong signature at the surface does not necessarily reflect their overall impact on ocean transport. The largest KE values associated with geostrophic currents essentially show the Gulf Stream evolution along the U.S. coasts and its eastward separation from the coast north of 35°N. The intrusion of the HB core over the AHNW region on 21 August 2009 increased the KE of the ageostrophic surface circulation, reaching high levels ($\sim$1 m^2/s^2) on 23 August, over the central AHNW region, where the HB core met the eastward flow associated with the Gulf Stream extension. Both total and ageostrophic KE were reduced on 24 August, when the HB core moved further north, away from the Gulf Stream surface front. The continuous increase of the total geostrophic KE over the extended AHNW region during the Gulf Stream evolution before the storm appearance (Fig. 20a) slowed down on 23 and 24 of August (HB passage) illustrating the distortion of the surface Gulf Stream by the storm. On the contrary, the total ageostrophic KE was relatively small before the HB intrusion and showed a significant peak on 23 August (>10,000 m^2/s^2) and strong reduction after the storm passage (Fig. 20b). The strong transport increase, computed after 26

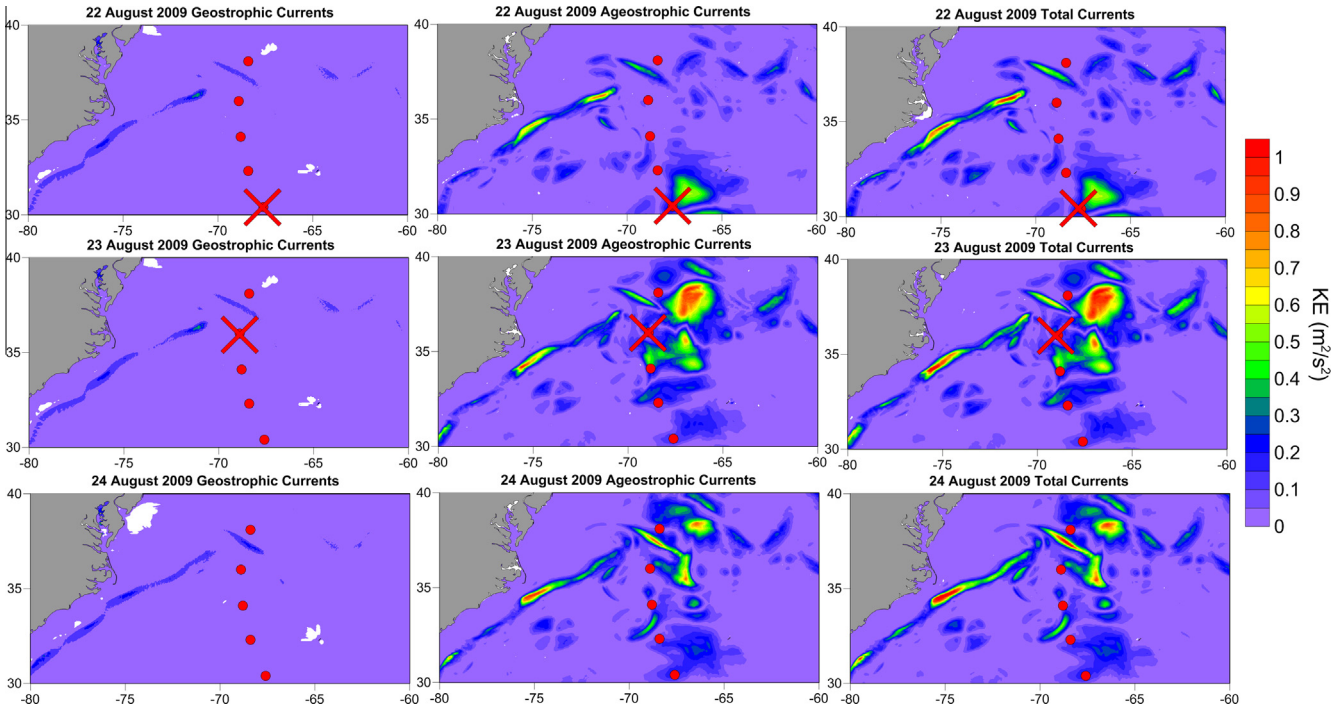

Fig. 19. Distribution of Kinetic Energy (KE, m^2/s^2) derived from surface geostrophic (left), ageostrophic (middle) and total (right) velocities (m/s) over the extended AHNW region (Fig. 1) on 22 (top), 23 (middle), 24 (bottom) August 2009. The Hurricane Bill (HB) track and the exact location of the HB core at each date are indicated with red circles (every 6 h at the hurricane core) and an "x" symbol, respectively. (For interpretation of the references to colour in this figure legend, the reader is referred to the web version of this article.)

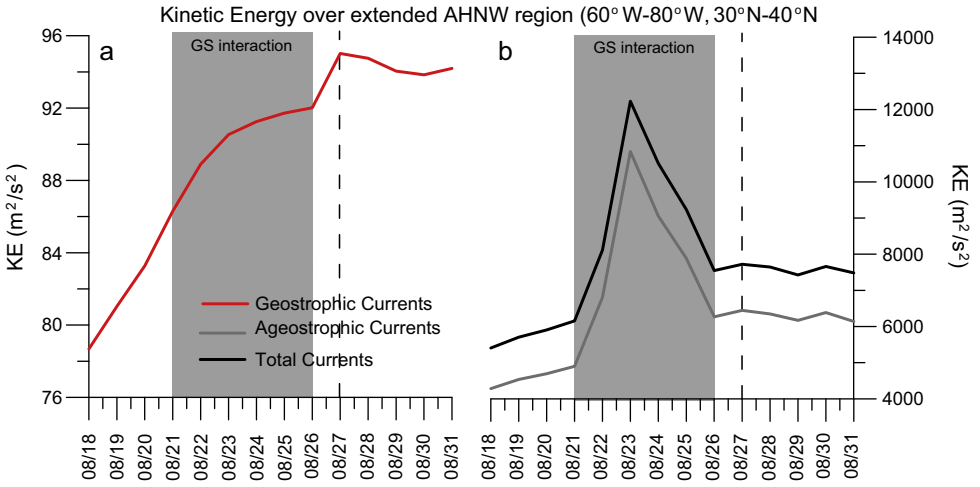

Fig. 20. Evolution of Kinetic Energy (KE, m^2/s^2) derived by simulated (a) geostrophic currents (red line) and (b) ageostrophic (grey line) and total (black line) currents, summed over the extended AHNW region (Fig. 1) from 18 August to 31 August 2009. The period of the hurricane's interaction with the Gulf Stream (GS) extension and the first day after Hurricane Bill (27 August) are indicated with a gray shaded area and a dashed line, respectively. (For interpretation of the references to colour in this figure legend, the reader is referred to the web version of this article.)

August (Fig. 15) is related to the restoration of the geostrophic circulation of the Gulf Stream propagation and not to the storm's induced ageostrophic circulation, which remained stable and in low levels after 26 August (Fig. 20b).

5. Conclusions

A high resolution application of the HYCOM for the North Atlantic Ocean hurricane region (ATL-HYCOM 0.04°) was implemented and a multi-year simulation was performed, with two objectives. The first is to evaluate a state-of-the-art, free-running simulation suitable for being the Nature Run (NR) in an ocean Observing System Simulation Experiments (OSSEs) framework. The NR task is to provide a source of synthetic observations, for performing OSSEs specifically designed to test the impact of measurements dedicated to improve the ocean component of coupled ocean-atmosphere hurricane prediction systems. The second objective is to use this simulation to investigate ocean-atmosphere interaction processes related to hurricane passages over the Atlantic Ocean. A specific example was chosen during the passage of Hurricane Bill (HB) in 2009.

The realism of the ATL-HYCOM 0.04° simulation was evaluated with respect to a wide variety of observations and processes. Comparisons with remotely sensed observations show the ability of the simulation to reproduce the mean dynamics, through comparison with altimetry, and the mean surface temperature and salinity structures of the basin. In addition, the model is able to reproduce the seasonal and inter-annual SST variations in four distinct sub-regions of the basin, dominated by different processes and circulation patterns (Atlantic Hurricane East and West regions, Equatorial region and Gulf Stream region). The realistic seasonal variations are also assessed for salinity, especially in the Equatorial region, despite the shorter satellite dataset. Comparisons with *in situ* surface temperature and salinity data at various moorings confirm the realism of the simulation for those quantities. The realistic representation of the main currents of the basin is confirmed by comparison with *in situ* near-surface drifter data, while the accuracy in the levels of simulated surface kinetic energy in the various sub-regions is assessed by comparison with estimates from altimetry (AVISO data). Below the surface, the difference in simulated temperature between the surface and 100 m depth is also found realistic at the seasonal time scale, when compared with the numerous Argo observations available in the basin; this is also true for salinity. As a result, the model computed stratification frequency in the upper 100 m also compares well with estimations from Argo data.

This evaluation leads to the conclusion that the ATL-HYCOM 0.04° simulation is well suited to represent the dominant processes affecting the North Atlantic Ocean hurricane region. In particular, the realism with which the simulation represents the Atlantic Ocean SST and its variability, which directly interact with hurricanes, and the variability in the upper ocean stratification, supports the use of this simulation as a Nature Run for performing OSSEs for testing observation networks dedicated to hurricane prediction systems. In addition, it is also suitable for performing process studies involving atmosphere-ocean interactions during the passage of a hurricane. A specific case study was demonstrated, examining the interaction between the HB passage in August 2009 and the Gulf Stream.

The passage of HB over the Atlantic Ocean was marked by an intense cold wake, reaching ~7 °C SST decrease in the Gulf Stream region, an effect that is well represented in the simulation. HB reached its maximum intensity (category 4 hurricane) around 21 August 2009, maintaining strong hurricane characteristics as it entered mid-latitudes and transitioned to extratropical status. In the Gulf Stream extension region, the HB passage was associated with a deepening of the Mixed Layer and a drop in stratification frequency consistent with observations. Moreover, the estimated eastward transport by the Gulf Stream over the top 100 m dropped drastically during the storm passage, due to opposing ageostrophic currents forced by the storm, and took a few days to recover its pre-storm level, as the ageostrophic flow was reduced. This is an important result, revealing a direct effect from a hurricane to the evolution of a western boundary current, which was not previously studied. Possible implications include variations in the feedback to the hurricane evolution, especially during the extratropical transition phase. Influence of the Gulf Stream to the evolution of extratropical storms has been previously documented, the most dramatic example associated with Hurricane Sandy in 2012. Changes in the Gulf Stream axis and extension (which we have shown can be induced by the hurricane passage) may, in return, influence hurricane evolution processes, such as the warm seclusion phase that was the case with Sandy's rapid intensification.

Our results showcased that the HB passage was accompanied by cells of cyclonic and anticyclonic near surface circulation, associated with the forced near-inertial wave wake, with cyclonic cells favoring the upwelling of deep, cold waters. We have shown that the hurricane passage interrupted the offshore signature of the Gulf Stream warm waters at the surface, likely resulting from the combined effects of local cooling and the interruption of warm water advection. Examination of the current kinematics indicates that the HB passage is associated with a pronounced increase in ageostrophic kinetic energy, directly forced by the storm, and a slowing down of the geostrophic kinetic energy, which then increases sharply after the passage of the storm. Our study thus illustrates how the passage of a hurricane can have a profound effect, which can last a few days, on the upper part of a western boundary current, such as the Gulf Stream. This is an important addition to previously studied processes of ocean feedbacks to hurricane intensification. Our results also showed that the model adequately simulated the upper-ocean response to all 13 hurricanes that propagated over the Gulf Stream extension region during the entire study period (2009–2014). All cases were characterized by significant increases in the mixed layer that eroded stratification, providing further evidence of substantial interaction between hurricanes and ocean properties over the Gulf Stream region.

This study had two important outcomes. The scientific aspect is that it provided a novel example of an atmospheric feedback to boundary current evolution. The technical aspect is that it presented the development and evaluation of a multi-year, high resolution simulation covering the Atlantic hurricane region. Such a simulation has the dual potential to be used for further studies of ocean-atmosphere interactions, and for observing system design. Given its ability in reproducing ocean conditions during the passage of an intense hurricane, this ATL-HYCOM 0.04° simulation is suitable to be used in the future as the Nature Run in OSSEs that can quantify the impact of various observation networks in reducing ocean model errors in a coupled ocean-atmosphere hurricane prediction context.

Acknowledgements

The authors acknowledge support from the NOAA Hurricane Sandy Disaster Relief Act (through award NA13OAR4830224) and from the NOAA Quantitative Observing System Assessment Program (QOSAP, P8R2W02PQF and NA15OAR4320064). G. Halliwell, M. Mehari, M. Le Hénaff and R. Lumpkin acknowledge support from NOAA's Atlantic Oceanographic and Meteorological Laboratory, Physical Oceanography Division. The altimeter products were produced by Ssalto/Duacs and distributed by Aviso (http://www.aviso.altimetry.fr/duacs/), with support from CNES (Centre National d'Etudes Spatiales). MDT_CNES-CLS13 was produced by CLS (Collecte Localisation Satellites) Space Oceanography Division and distributed by Aviso (http://www.aviso.altimetry.fr/), with support from CNES. We thank Alan Wallcraft (NRL-SSC) for preparing the GDEM42 climatology for our project.

References

Androulidakis, Y.S., Kourafalou, V.H., Halliwell, G.R., Kang, H., Mehari, M., Le Hénaff, M., Atlas, R., 2016. Hurricane interaction with the upper-ocean in the Amazon-Orinoco plume region. Ocean Dynamics (accepted for publication).

Archer, C., Baptista, A., Leen, T.K., 2003. Fault detection for salinity sensors in the Columbia estuary. Water Resources Research 39 (3).

Arnault, S., Bourles, B., Gouriou, Y., Chuchla, R., 1999. Intercomparison of upper layer circulation of the western equatorial Atlantic Ocean: in situ and satellite data. Journal of Geophysical Research 104 (C9), 21171–21194.

Atlas, R., 1997. Atmospheric observations and experiments to assess their usefulness in data assimilation. J. Meteor. Soc. Jpn. 75, 111–130.

Atlas, R., Emmitt, G.D., 2008. Review of observing system simulation experiments to evaluate the potential impact of lidar winds on numerical weather prediction. ILRC24 2, 726–729 (ISBN 978-0-615-21489-4).

Auer, S.J., 1987. Five-year climatological survey of the Gulf Stream system and its associated rings. Journal of Geophysical Research 92 (C11), 11709–11726.

Avila, L.A., 2010. Hurricane Bill Tropical Cyclone Report. National Hurricane Center. January 18, 2010. Available On Line: <http://www.nhc.noaa.gov/data/tcr/AL032009_Bill.pdf>.

Bauer, R., 1982. Functional Description: Master Oceanographic Observation Data Set (MOODS). Compass System Inc., San Diego, CA.
Beckmann, A., Böning, C.W., Köberle, C., Willebrand, J., 1994. Effects of increased horizontal resolution in a simulation of the North Atlantic Ocean. Journal of Physical Oceanography 24, 326–344.
Bender, M., Ginis, I., Tuleya, R., Thomas, B., Marchok, T., 2007. The operational GFDL coupled hurricane-ocean prediction system and a summary of its performance. Monthly Weather Review 135, 3965–3989.
Berg, R.J., Avila, L.A., 2010. Atlantic hurricane season of 2009. Monthly Weather Review 139 (4), 1049–1069. http://dx.doi.org/10.1175/2010mwr3476.1.
Bleck, R., 2002. An oceanic general circulation model framed in hybrid isopycnic Cartesian coordinates. Ocean Modelling 4 (1), 55–88.
Bleck, R., Halliwell, G., Wallcraft, A., Carrol, S., Kelly, K., Rushing, K., 2002. Hybrid Coordinate Ocean Model (HYCOM). User's Manual, 199 pp.
Bosart, L., Velden, C.S., Bracken, W.E., Molinari, J., Black, P.G., 2000. Environmental influences on the rapid intensi- fication of Hurricane Opal (1995) over the Gulf of Mexico. Monthly Weather Review 128, 322–352.
Bourles, B., Gouriou, Y., Chuchla, R., 1999. On the circulation and upper layer of the western equatorial Atlantic. Journal of Geophysical Research 104 (C9), 21151–21170.
Boyer, T.P., Antonov, J.I., Gracia, H.E., Johnson, D.R., Locarnini, R.A., Mishonov, A.V., Pitcher, M.T., Baranova, O.K., Smolyar, I.V., 2006. World Ocean Database 2005. In: Levitus, S. (Ed.), NOAA Atlas NESDIS 60. U.S Government Printing Office, Washington, D.C.. 190 pp.
Bright, R.J., Xie, L., Pietrafesa, L.J., 2002. Evidence of the Gulf Stream's influence on tropical cyclone intensity. Geophysical Research Letters 29 (16), 1801. http://dx.doi.org/10.1029/2002GL014920.
Bryan, F.O., Holland, W.R., 1989. A high resolution simulation of the wind-and thermohaline-driven circulation in the North Atlantic Ocean. In: Parameterization of Small-Scale Processes in the Ocean, Proceedings of the Hawaiian Winter Workshop. University of Hawaii, pp. 99–115.
Carnes, M.R., 2010. Validation Test Report for GDEM4 NRL Memorandum 7330-10-9271, 59 pp.
Chassignet, E.P., Smith, L.T., Halliwell, G.R., Bleck, R., 2003. North Atlantic simulations with the Hybrid Coordinate Ocean Model (HYCOM): impact of the vertical coordinate choice, reference pressure, and thermobaricity. Journal of Physical Oceanography 33 (12), 2504–2526.
Chassignet, E.P., Hurlburt, H.E., Smedstad, O.M., Halliwell, G.R., Hogan, P.J., Wallcraft, A.J., Baraille, R., Bleck, R., 2007. The HYCOM (Hybrid Coordinate Ocean Model) data assimilative system. Journal of Marine Systems 65 (1), 60–83.
Condie, S.A., 1991. Separation and recirculation of the North Brazil Current. Journal of Marine Research 49 (1), 1–19.
D'Asaro, E.A., Sanford, T.B., Niiler, P.P., Terrill, E.J., 2007. Cold wake of hurricane Francis. Geophysical Research Letters 34 (L15609). http://dx.doi.org/10.1029/2007GL030160.
Delcroix, T., Dessier, A., Gouriou, Y., McPhaden, M., 2005. Time and space scales for sea surface salinity in the tropical oceans. Deep Sea Research Part I 52, 787–813.
DeMaria, M., Kaplan, J., 1994. Sea surface temperature and the maximum intensity of Atlantic tropical cyclones. Journal of Climate 7 (9), 1324–1334.
Diakakis, M., Deligiannakis, G., Katsetsiadou, K., Lekkas, E., 2015. Hurricane Sandy mortality in the Caribbean and continental North America. Disaster Prevention and Management 24 (1), 132–148. http://dx.doi.org/10.1108/DPM-05-2014-0082.
Donlon, C.J., Casey, K.S., Robinson, I.S., Gentemann, C.L., Reynolds, R.W., Barton, I., Minnett, P., 2003. The GODAE High Resolution Sea Surface Temperature Pilot Project (GHRSST-PP). EGS-AGU-EUG Joint Assembly 1, 1636.
Elsberry, R.L., Lambert, T.D., Boothe, M.A., 2007. Accuracy of Atlantic and eastern North Pacific tropical cyclone intensity forecast guidance. Weather and Forecasting 22 (4), 747–762.
Emanuel, K.A., 1999. Thermodynamic control of hurricane intensity. Nature 401 (6754), 665–669.
Fisher, E.L., 1958. Hurricanes and the sea-surface temperature field. Journal of Meteorology 15 (3), 328–333.
Frankignoul, C., de Coëtlogon, G., Joyce, T.M., Dong, S.F., 2001. Gulf stream variability and ocean-atmosphere interactions. Journal of Physical Oceanography 31 (12), 3516–3529.
Fratantoni, D.M., 2001. North Atlantic surface circulation during the 1990's observed with satellite-tracked drifters. Journal of Geophysical Research 106, 22067–22093.
Fuglister, F.C., Voorhis, A.D., 1965. A new method of tracking the Gulf Stream. Limnology and Oceanography 10 (suppl), R115–R124.
Galarneau Jr., J.T., Davis, C.A., Shapiro, M.A., 2013. Intensification of Hurricane Sandy (2012) through Extratropical Warm Core Seclusion. Monthly Weather Review 141 (12), 4296–4321.
Gentemann, C.L., Wentz, F.J., DeMaria, M., 2006. Near real time global optimum interpolated microwave SSTs: applications to hurricane intensity forecasting. In: 27th conference on hurricanes and tropical meteorology, Monterey, CA.
Gierach, M.M., Vazquez-Cuervo, J., Lee, T., Tsontos, V.M., 2013. Aquarius and SMOS detect effects of an extreme Mississippi River flooding event in the Gulf of Mexico. Geophysical Research Letters 40 (19), 5188–5193.
Gordon, A.L., Giulivi, C.F., 2014. Ocean eddy freshwater flux convergence into the North Atlantic subtropics. Journal of Geophysical Research: Oceans 119 (6), 3327–3335.
Grodsky, S.A., Reul, N., Lagerloef, G., Reverdin, G., Carton, J.A., Chapron, B., Quilfen, Y., Kudryavtsev, V.N., Kao, H.-Y., 2012. Haline hurricane wake in the Amazon/Orinoco plume: AQUARIUS/SACD and SMOS observations. Geophysical Research Letters 39 (20), L20603.
Grodsky, S.A., Reverdin, G., Carton, J.A., Coles, V.J., 2014. Year-to-year salinity changes in the Amazon plume: Contrasting 2011 and 2012 Aquarius/SACD and SMOS satellite data. Remote Sensing of Environment 140, 14–22.
Halkin, D., Rossby, T., 1985. The structure and transport of the Gulf Stream at 73 W. Journal of Physical Oceanography 15 (11), 1439–1452.
Halliwell, G.R., 2004. Evaluation of vertical coordinate and vertical mixing algorithms in the HYbrid-Coordinate Ocean Model (HYCOM). Ocean Modelling 7 (3), 285–322.
Halliwell, G.R., Srinivasan, A., Kourafalou, V.H., Yang, H., Willey, D., Le Hénaff, M., Atlas, R., 2014. Rigorous Evaluation of a Fraternal Twin Ocean OSSE System for the Open Gulf of Mexico. Journal of Atmospheric and Oceanic Technology 31 (1), 105–130. http://dx.doi.org/10.1175/JTECH-D-13-00011.1.
Halliwell, G.R., Kourafalou, V.H., Le Hénaff, M., Shay, L.K., Atlas, R., 2015. OSSE impact analysis of airborne ocean surveys for improving upper ocean dynamical and thermodynamical forecasts in the Gulf of Mexico. Progress in Oceanography. http://dx.doi.org/10.1016/j.pocean.2014.09.004.
Halliwell, G.R., Mehari, M., Le Hénaff, M., Kourafalou, V.H., Androulidakis, Y.S., Kang, H., Atlas, R., 2016. OSSE evaluation of the operational ocean observing system and supplemental seasonal observations for improving coupled tropical cyclone prediction. Journal of Operational Oceanography (submitted for publication).
Hansen, D.V., Maul, G.A., 1970. A note on the use of sea surface temperature for observing ocean currents. Remote Sensing of the Environment 1 (3), 161–164.
Hernandez, O., Boutin, J., Kolodziejczyk, N., Reverdin, G., Martin, N., Gaillard, F., Reul, N., Vergely, J.L., 2014. SMOS salinity in the subtropical North Atlantic salinity maximum: 1. Comparison with Aquarius and in situ salinity. Journal of Geophysical Research: Oceans 119 (12), 8878–8896. http://dx.doi.org/10.1002/2013JC009610.
Horton, C.W., 1984. Surface front displacement in the Gulf Stream by hurricane/tropical storm Dennis. Journal of Geophysical Research: Oceans 89 (C2), 2005–2012.
Jaimes, B., Shay, L.K., 2010. Near-inertial wave wake of Hurricanes Katrina and Rita over mesoscale oceanic eddies. Journal of Physical Oceanography 40 (6), 1320–1337.
Jaimes, B., Shay, L.K., 2015. Enhanced wind-driven downwelling flow in warm oceanic eddy features during the intensification of tropical cyclone Isaac (2012): observations and theory. Journal of Physical Oceanography 45, 1667–1689.
Johns, W.E., Shay, T.J., Bane, J.M., Watts, D.R., 1995. Gulf Stream structure, transport, and recirculation near 68 W. Journal of Geophysical Research 100. 817–817.
Jouanno, J., Sheinbaum, J., Barnier, B., Molines, J.M., Debreu, L., Lemarié, F., 2008. The mesoscale variability in the Caribbean Sea. Part I: Simulations and characteristics with an embedded model. Ocean Modelling 23 (3), 82–101.
Jugan, M.J., Beresford, H., 1991. Editing Approach for the Navy's Master Oceanographic Observation Data Set, Published in Proceedings of MTS'91, An Ocean Cooperative: Industry, Government, and Academia, VOL. II, 1164.
Kaplan, J., DeMaria, M., Knaff, J.A., 2010. A revised tropical cyclone rapid intensification index for the Atlantic and eastern North Pacific basins. Weather and Forecasting 25 (1), 220–241.
Kara, A.B., Wallcraft, A.J., Hurlburt, H.E., 2005. Sea surface temperature sensitivity to water turbidity from simulations of the Turbid Black Sea using HYCOM. Journal of Physical Oceanography 35 (1), 33–54.
Kelly, K.A., Gille, S.T., 1990. Gulf Stream surface transport and statistics at 69°W. Journal of Geophysical Research 95 (C3), 3149–3161.
Knauss, J.A., 1969. A note on the transport of the Gulf Stream. Deep-Sea Research 16, 117–123.
Kourafalou, V.H., Oey, L.-Y., Lee, T.N., Wang, J.D., 1996. The fate of river discharge on the continental shelf. Part II: transport of low-salinity waters under realistic wind and tidal forcing. Journal of Geophysical Research 101 (C2), 3435–3455. http://dx.doi.org/10.1029/95JC03025.
Kourafalou, V.H., Kang, H., 2012. Florida Current meandering and evolution of cyclonic eddies along the Florida Keys Reef Tract: are they inter-connected? Journal of Geophysical Research 117, C05028. http://dx.doi.org/10.1029/2011JC007383.
Kourafalou, V.H., Androulidakis, Y.S., 2013. Influence of Mississippi River induced circulation on the Deepwater Horizon oil spill transport. Journal of Geophysical Research: Oceans 118 (8), 3823–3842.
Kourafalou, V.H., De Mey, P., Le Hénaff, M., Charria, G., Edwards, C.A., He, R., Herzfeld, M., Pasqual, A., Stanev, E., Tintoré, J., Usui, N., Van Der Westhuysen, A., Wilkin, J., Zhu, X., 2015. Coastal Ocean Forecasting: system integration and validation. Journal of Operational Oceanography. http://dx.doi.org/10.1080/1755876X.2015.1022336.
Lagerloef, G., Colomb, F.R., Le Vine, D., Wentz, F., Yueh, S., Ruf, C., Lilly, J., Gunn, J., Chao, Y., deCharon, A., Feldman, G., Swift, C., 2008. The Aquarius/SAC-D mission: designed to meet the salinity remote-sensing challenge. Oceanography 21, 68–81. http://dx.doi.org/10.5670/oceanog.2008.68.
Lagerloef, G., 2012. Satellite mission monitors ocean surface salinity. Eos Trans. AGU 93 (25), 233. http://dx.doi.org/10.1029/2012EO250001.
Lagerloef, G., Wentz, F., Yueh, S., Kao, H.-Y., Johnson, G.C., Lyman, J.M., 2012. Aquarius satellite mission provides new, detailed view of sea surface salinity. In: State of the Climate in 2011, Bulletin of the American Meteorological Society, vol. 93, Boston, Mass, pp. S70–S71.
Landsea, C.W., Anderson, C., Charles, N., Clark, G., Dunion, J., Fernandez-Partagas, J., Hungerford, P., Neumann, C., Zimmer, M., 2004. The Atlantic hurricane database re-analysis project: Documentation for the 1851–1910 alterations and

additions to the HURDAT database. Hurricanes and Typhoons: Past, Present and Future, 177–221.
Landsea, C.W., 1993. A climatology of intense (or major) Atlantic hurricanes. Monthly Weather Review 121 (6), 1703–1713.
Large, W.G., McWilliams, J.C., Doney, S.C., 1994. Oceanic vertical mixing: a review and a model with a nonlocal boundary layer parameterization. Reviews of Geophysics 32 (4), 363–404.
Le Hénaff, M., Kourafalou, V.H., 2016. Mississippi waters reaching South Florida reefs under no flood conditions: synthesis of observing and modeling system findings. Ocean Dynamics 66, 435–459.
Le Hénaff, M., Kourafalou, V.H., Morel, Y., Srinivasan, A., 2012. Simulating the dynamics and intensification of cyclonic Loop Current Frontal Eddies in the Gulf of Mexico. Journal of Geophysical Research: Oceans (1978–2012) 117 (C2).
Leaman, K.D., Molinari, R.L., Vertes, P.S., 1987. Structure and variability of the Florida Current at 27 N: April 1982-July 1984. Journal of Physical Oceanography 17 (5), 565–583.
Leipper, D., Volgenau, D., 1972. Upper ocean heat content of the Gulf of Mexico. Journal of Physical Oceanography 2, 218–224.
Lentz, S.J., 1995. Seasonal variations in the horizontal structure of the Amazon Plume inferred from historical hydrographic data. Journal of Geophysical Research 100, 2391–2400. http://dx.doi.org/10.1029/94JC01847.
Lewis, K., Allen, J.I., 2009. Validation of a hydrodynamic-ecosystem model simulation with time-series data collected in the western English Channel. Journal of Marine Systems 77 (3), 296–311.
Lloyd, I.D., Vecchi, G.A., 2011. Observational evidence for oceanic controls on hurricane intensity. Journal of Climate 24, 1138–1153. http://dx.doi.org/10.1175/2010JCLI3763.1.
Lumpkin, R., 2003. Decomposition of surface drifter observations in the Atlantic Ocean. Geophysical Research Letters 30 (14), 1753. http://dx.doi.org/10.1029/2003GL017519.
Lumpkin, R., Johnson, G.C., 2013. Global ocean surface velocities from drifters: mean, variance, El Niño-Southern Oscillation response, and seasonal cycle. Journal of Geophysical Research: Oceans 118 (6), 2992–3006.
Mehra, A., Rivin, L., 2010. A real time ocean forecast system for the North Atlantic Ocean. Terrestrial, Atmospheric and Oceanic Sciences 21 (1), 211–228.
Nguyen, L.T., Molinari, J., 2012. Rapid intensification of a sheared, fast-moving hurricane over the Gulf Stream. Monthly Weather Review 140 (10), 3361–3378.
Oey, L.Y., Ezer, T., Wang, D.P., Fan, S.J., Yin, X.Q., 2006. Loop current warming by Hurricane Wilma. Geophysical Research Letters 33 (8), L08613.
Oke, P.R., Larnicol, G., Jones, E.M., Kourafalou, V.H., Sperrevik, A.K., Carse, F., Tanajura, C.A.S., Mourre, B., Tonani, M., Brassington, G.B., Le Hénaff, M., Halliwell, G.R., Atlas, R., Moore, A.M., Edwards, C.A., Martin, M.J., Stellar, A.A., Alvarez, A., De Mey, P., Iskandarani, M., 2015. Assessing the impact of observations on ocean forecasts and reanalyses: Part 2: Regional applications. Journal of Operational Oceanography. http://dx.doi.org/10.1080/1755876X.2015.1022080.
Pearson, K., 1903. Mathematical contributions to the theory of evolution. XI. On the influence of natural selection on the variability and correlation of organs. Philosophical Transactions of the Royal Society of London 200, 1–66.
Price, J.F., 1981. Upper ocean response to a hurricane. Journal of Physical Oceanography 11 (2), 153–175.
Price, J.F., 2009. Metrics of hurricane-ocean interaction: vertically-integrated or vertically-averaged ocean temperature? Ocean Science 5, 351–368.
Reverdin, G., Kestenare, E., Frankignoul, C., Delcroix, T., 2007. Surface salinity in the Atlantic Ocean (30S–50N). Progress in Oceanography 73, 311–340.
Samson, G., Giordani, H., Caniaux, G., Roux, F., 2009. Numerical investigation of an oceanic resonant regime induced by hurricane winds. Ocean Dynamics 59 (4), 565–586.
Schade, L.R., Emanuel, K.A., 1999. The ocean's effect on the intensity of tropical cyclones: results from a simple coupled atmosphere-ocean model. Journal Atmospheric Science 56, 642–651.
Schiller, R.V., Kourafalou, V.H., 2010. Modeling river plume dynamics with the HYbrid Coordinate Ocean Model. Ocean Modelling 33 (1), 101–117.
Scoccimarro, E., Gualdi, S., Bellucci, A., Sanna, A., Fogli, P.G., Manzini, E., Vichi, M., Oddo, P., Navarra, A., 2011. Effects of tropical cyclones on ocean heat transport in a high resolution coupled general circulation model. Journal of Climate 24, 4368–4384. http://dx.doi.org/10.1175/2011JCLI4104.1.
Shay, L.K., Goni, G.J., Black, P.G., 2000. Effects of a warm oceanic feature on Hurricane Opal. Monthly Weather Review 128 (5), 1366–1383.
Shay, L.K., Mariano, A.J., Jacob, S.D., Ryan, E.H., 1998. Mean and near-inertial ocean current response to Hurricane Gilbert. Journal of Physical Oceanography 28 (5), 858–889.
Simon, E., Bertino, L., 2009. Application of the Gaussian anamorphosis to assimilation in a 3-D coupled physical-ecosystem model of the North Atlantic with the EnKF: a twin experiment. Ocean Science 5 (4), 495–510.
Steel, R.G.D., Torrie, J.H., 1960. Principles and Procedures of Statistics with Special Reference to the Biological Sciences. McGraw-Hill, New York, USA.
Tang, W., Yueh, S.H., Fore, A.G., Hayashi, A., 2014. Validation of Aquarius sea surface salinity with in situ measurements from Argo floats and moored buoys. Journal of Geophysical Research: Oceans 119 (9), 6171–6189.
Walker, N.D., Leben, R.R., Balasubramanian, S., 2005. Hurricane-forced upwelling and chlorophyll a enhancement within cold-core cyclones in the Gulf of Mexico. Geophysical Research Letters 32 (18), L18610.
Willmott, C.J., 1981. On the validation of models. Physical Geography 2 (2), 184–194.
Winther, N.G., Evensen, G., 2006. A hybrid coordinate ocean model for shelf sea simulation. Ocean Modelling 13 (3), 221–237.
Zamudio, L., Hogan, P.J., 2008. Nesting the Gulf of Mexico in Atlantic HYCOM: oceanographic processes generated by Hurricane Ivan. Ocean Modelling 21 (3), 106–125.